NAVAL POSTGRADUATE SCHOOL
Monterey, California

THESIS

A MODAL APPROXIMATION FOR THE MUTUAL RADIATION IMPEDANCE FOR SHPERICAL SOURCES AND ACOUSTIC WAVE SCATTERING USING AN IMPROVED ATILA FINITE ELEMENT CODE

by

Joseph L. Day

September 1999

Thesis Advisor: Clyde L. Scandrett
Co-Advisor: Steven R. Baker

Approved for public release; distribution is unlimited.

REPORT DOCUMENTATION PAGE

Form Approved OMB No. 0704-0188

1. AGENCY USE ONLY *(Leave blank)*	2. REPORT DATE	3. REPORT TYPE AND DATES COVERED
	September 1999	Master's Thesis

4. TITLE AND SUBTITLE
A MODAL APPROXIMATION FOR THE MUTUAL RADIATION IMPEDANCE FOR SPHERICAL SOURCES AND ACOUSTIC WAVE SCATTERING USING AN IMPROVED ATILA FINITE ELEMENT CODE

5. FUNDING NUMBERS

6. AUTHOR(S)
Day, Joseph L.

7. PERFORMING ORGANIZATION NAME(S) AND ADDRESS(ES)
Naval Postgraduate School
Monterey, CA 93943-5000

8. PERFORMING ORGANIZATION REPORT NUMBER

9. SPONSORING / MONITORING AGENCY NAME(S) AND ADDRESS(ES)

10. SPONSORING / MONITORING AGENCY REPORT NUMBER

11. SUPPLEMENTARY NOTES
The views expressed in this thesis are those of the author and do not reflect the official policy or position of the Department of Defense or the U.S. Government.

12a. DISTRIBUTION / AVAILABILITY STATEMENT
Approved for public release; distribution is unlimited.

12b. DISTRIBUTION CODE

13. ABSTRACT *(maximum 200 words)*

A modal approximation for the self and mutual radiation impedances has been derived for arrays of spherical transducers with small *ka* values, where *ka* is the acoustic wave number multiplied by the radius of the sphere. I term this the "Modal Pritchard" approximation, as it is related to the so-called Pritchard approximation, often employed to calculate mutual radiation impedances. I investigated the utility of the approximate mutual radiation impedance expression for three two-body problems (monopoles, aligned dipoles, and aligned-linear quadrupoles). For these cases, approximate values were found to be in good agreement with those obtained using a full Spherical Addition Theorem calculation, and are an improvement over the simple Pritchard approximation. Additionally, I investigated the mutual radiation impedance expression in one particular three-body problem. Because of the Modal Pritchard approximation's inability to correctly handle scattering, we recommend using the full Spherical Addition Theorem calculation when scattering is important.

Finally, I investigated the use of a new finite element mesh to calculate the T-matrix for a given transducer. The T-matrix relates the incident and scattered waves for a single transducer, in an orthogonal (spherical harmonic) basis set. The monopole element showed an increase in error, while we saw some improvements in the higher-order diagonal elements. Off-diagonal elements, which should be zero for a spherical scatter, were satisfactorily small in most cases. Although the results were less than favorable, I was able to streamline the T-matrix calculation while providing a new method of examining the off-diagonal elements.

14. SUBJECT TERMS
ATILA-finite element code, mutual and self radiation impedance, and normal mode spherical harmonics

15. NUMBER OF PAGES
97

16. PRICE CODE

17. SECURITY CLASSIFICATION OF REPORT	18. SECURITY CLASSIFICATION OF THIS PAGE	19. SECURITY CLASSIFI- CATION OF ABSTRACT	20. LIMITATION OF ABSTRACT
Unclassified	Unclassified	Unclassified	UL

NSN 7540-01-280-5500

Standard Form 298 (Rev. 2-89)
Prescribed by ANSI Std. 239-18

Approved for public release; distribution is unlimited

A MODAL APPROXIMATION FOR THE MUTUAL RADIATION IMPEDANCE FOR SPHERICAL SOURCES AND ACOUSTIC WAVE SCATTERING USING AN IMPROVED ATILA FINITE ELEMENT CODE

Joseph L. Day
B.S., University of Texas – El Paso, 1990

Submitted in partial fulfillment of the
requirements for the degree of

MASTER OF SCIENCE IN ENGINEERING ACOUSTICS

from the

NAVAL POSTGRADUATE SCHOOL
September 1999

Author: Joseph L. Day
Joseph L. Day

Approved by:
Clyde L. Scandrett, Thesis Advisor

Steven R. Baker, Co-Advisor

Kevin B. Smith, Chairman
Engineering Acoustics Academic Committe

ABSTRACT

A modal approximation for the self and mutual radiation impedances has been derived for arrays of spherical transducers with small *ka* values, where *ka* is the acoustic wave number multiplied by the radius of the sphere. I term this the "Modal Pritchard" approximation, as it is related to the so-called Pritchard approximation, often employed to calculate mutual radiation impedances. I investigated the utility of the approximate mutual radiation impedance expression for three two-body problems (monopoles, aligned dipoles, and aligned-linear quadrupoles). For these cases, approximate values were found to be in good agreement with those obtained using a full Spherical Addition Theorem calculation, and are an improvement over the simple Pritchard approximation. Additionally, I investigated the mutual radiation impedance expression in one particular three-body problem. Because of the Modal Pritchard approximation's inability to correctly handle scattering, we recommend using the full Spherical Addition Theorem calculation when scattering is important.

Finally, I investigated the use of a new finite element mesh to calculate the T-matrix for a given transducer. The T-matrix relates the incident and scattered waves for a single transducer, in an orthogonal (spherical harmonic) basis set. The monopole element showed an increase in

error, while we saw some improvements in the higher-order diagonal elements. Off-diagonal elements, which should be zero for a spherical scatter, were satisfactorily small in most cases. Although the results were less than favorable, I was able to streamline the T-matrix calculation while providing a new method of examining the off-diagonal elements.

TABLE OF CONTENTS

ACKNOWLEDGMENTS

I would like to thank several individuals that have helped me during the past two years. I would first like to thank the personnel of the professional development directorate at the Office of Naval Intelligence (ONI) and the personnel of Code 34 at the Naval Postgraduate School, namely, Linda Colvin and Gigi Verbos of ONI and Eva Anderson, Gale Johnson, and Pam Silva of NPS. These people totally eliminated any and all administrative concerns allowing me to concentrate exclusively on my academic endeavors.

Next I would like to thank the faculty of the Physics, Mathematics, and Engineering Departments at NPS, namely my two thesis advisors: Clyde Scandrett of the Mathematics Department and Steven Baker of the Physics Department. No matter how many times I knocked on Professor Scandrett's door there was always a cheerful "come in" response. I appreciate both of these men and their willingness to allow me to participate in their important work for one of the U.S. Navy's laboratories.

Finally, I would like to thank my wife, Kim, for her continued support of me and dedication to our two children, Christina and Eric.

I. INTRODUCTION

The work described in this thesis is part of an ongoing effort to improve our ability to accurately model densely packed underwater acoustic arrays. When an acoustic array's operating characteristics are closely predicted we say the array behaves well. This behavior is influenced by element interaction, characterized by a parameter called mutual radiation impedance (Ref. 1). A worst case example of "bad" behavior is that a transducer element may actually absorb acoustic power, which is then absorbed back into the driving amplifier, thus possibly causing an overload and electrical failure (Ref. 2). Other examples of bad behavior include changes in the radiated source level and deviations of the beampattern, steering direction, and side lobe amplitudes.

Element-to-element interactions are more significant in arrays that are packed into a volume of small size, which is the trend in low frequency active arrays. We will analyze the mutual radiation impedance for spherical sources of small ka values, where k is the wave number and a is the radius of the sphere. The mutual radiation impedance is an important parameter used to calculate the pressure on one array transducer due to the radiation and scattering from other transducers in the array.

Additionally, I will use a finite element code to solve for the radiating and scattering properties of a single

transducer. Therefore, this thesis consists of two portions.

The first part is devoted to deriving a general expression for the mutual radiation impedance between two identical radiating hard spheres in an otherwise free field environment using a normal mode approach. Additionally, an expression for the self-radiation impedance, which is the radiation loading on a single element in a free field, is found.

I have compared our modal approximation for the mutual radiation impedance with the commonly-used so-called "Pritchard" approximation for the particular case $ka = 1$, and will show the improvement possible using our modal approximation. This improvement is particularly noticeable as the center-to-center distance between sources is reduced. In this "Simple Pritchard" approximation, as I refer to it, the real part of the self-radiation impedance is multiplied by a spherical Hankel function of zeroth order to find the mutual radiation impedance. I will show how this "simple" approximation starts to break down as the transducers are spatially brought closer together.

The Addition Theorem (Ref. 3) provides one the ability to mathematically express the pressure radiated from one body referenced to the coordinate system of another body. Using the Addition Theorem, it is possible to very

accurately compute the mutual radiation impedance of a sphere in an arbitrarily densely packed array of any number of elements. I have used the Addition Theorem as a computational standard.

I also applied our modal approximation to a specified three-body problem to further investigate our modal approximation, which I will hereafter refer to as the "Modal Pritchard" approximation. In this problem we note the inability of our Modal Pritchard approximation to handle the effects of scattering. Because of this breakdown we recommend using the full Spherical Addition Theorem for this problem and other cases when scattering becomes important. Methods and computer codes for this portion of the thesis are provided in Appendixes A and B.

The second part of this thesis makes extensive use of a finite element code, named ATILA, which was written by engineers at the Institut Superieur d'Electronique du Nord (ISEN). ATILA has been specifically developed to aid in the design of sonar transducers, but is also used to model a variety of acoustic problems.

The final portion of this thesis addresses the T-matrix method (Ref. 3). In order to model certain aspects of array operation such as near-field pressure, it is necessary to solve for the radiating and scattering properties of a single transducer. We accomplish this calculation by using

the ATILA finite element code. The T-Matrix (or Transition Matrix) characterizes the scattering properties of a specific body by translating incoming pressure waves to outgoing ones.

I will provide a brief description of ATILA's method of calculation that distinguishes it from other finite element codes. Readers less familiar with finite element codes may want to seek further information from reference books such as Kwon's "The Finite Element Method using MATLAB" (Ref. 4).

Previous work with ATILA to calculate the T-matrix for a thin-spherical shell has been shown to be in error when compared with a verified analytical solution (Ref. 5). Various limitations of the ATILA code may explain the errors present. I investigated whether improvements are obtained by making some corrections to ATILA's code and by the implementation of a new, refined, finite element mesh. This new mesh increased the errors to the monopole element but did provide some improvement to other T-matrix elements. Further improvements may be realized with the advent of more sophisticated radiation boundary operators. An early delivery of an addition to the ATILA code, EQI, which uses using a boundary element method to handle the fluid, did not occur in time for use with this thesis. Investigation of the improvement obtained using ATILA coupled with EQI will have to be the subject of future research.

In addition to providing some improvement in the calculation of the T-matrix, I have been able to streamline the procedure. Output scattered pressures from ATILA were post-processed using easy to read MATLAB program scripts. The resulting T-matrix calculations were quickly compared with the analytical results (also done in MATLAB). Listed in Appendix C are the MATLAB codes used to calculate the theoretical values of the T-matrix elements and the T-matrix elements calculated from ATILA's scattered pressure results.

In summary, by deriving an improved analytical formulation for the mutual radiation impedance, one can quickly investigate the effects of parameter variations, such as the distance between elements in the array. Additionally since this formulation involves angular dependence, I have devised a means of investigating the effects of altering the orientation between elements in an array. We recommend using the Modal Pritchard approximation for approximate solutions when scattering is unimportant, and the full spherical Addition Theorem otherwise. Streamlining the T-matrix calculation for a given transducer will allow follow-on work to be accomplished with less startup time.

(THIS PAGE INTENTIONALLY LEFT BLANK)

II. THEORETICAL BACKGROUND SECTION

This chapter addresses the development of a modal approximation for the self and mutual radiation impedances for two spheres in an otherwise free field environment.

A. BOUNDARY CONDITIONS

Consider a space and time dependent velocity potential, defined as $\Psi(\boldsymbol{r},t) = \Psi(\boldsymbol{r})e^{j\omega t}$, where the vector $\boldsymbol{r} = (r,\theta,\phi)$ represents the spatial dependence. A relationship between the pressure (p) and the velocity potential (Ψ) states $p = -\rho_o \partial\Psi/\partial t$ (Ref. 6), so that $p = -j\omega\rho_o\Psi$.

Taking the gradient and then the dot product with the radial unit vector, we obtain $\partial\Psi/\partial r = -1/(j\omega\rho_o)\ \partial p/\partial r$. By noting that the velocity vector is defined to equal the gradient of the velocity potential ($\boldsymbol{u} = \nabla\Psi$), we can derive a boundary condition for a surface normal velocity. For a sphere of radius a, for example, evaluation of $\partial\Psi/\partial r = -1/(j\omega\rho_o)\partial p/\partial r$ at $r=a$ provides an expression for the radial velocity on the sphere's surface. This will be a boundary condition for our analysis.

$$V_{radial}\Big|_{r=a} = \frac{j}{\omega\rho_o}\frac{\partial p}{\partial r}\Big|_{r=a} \qquad (1)$$

B. PROBLEM SETUP AND ADDITION THEOREM

Consider two identical spheres (radii = a) spaced with a center-to-center distance = d. Letting (r_1, θ_1, ϕ_1) and (r_2, θ_2, ϕ_2) be the spherical coordinates relative to the centers of spheres one and two, respectively. With the two spheres radiating in distinct normal modes, the radial velocities are expressed below.

$$V_1 = V_{n1}^{m1}\,\Omega_{n1}^{m1}(\theta_1, \phi_1)$$
$$V_2 = V_{n2}^{m2}\,\Omega_{n2}^{m2}(\theta_2, \phi_2) \qquad (2)$$

Where $\Omega_n^m = P_n^m(\cos\theta)e^{jm\phi}$ is a modal eigenfunction, P_n^m is the Legendre function, and V_{n1}^{m1} *and* V_{n2}^{m2} are modal amplitudes.

The pressure from each sphere can be mathematically expressed as shown in Equation (3) (Ref. 3). Since we are assuming a $e^{j\omega t}$ time dependence, we use a spherical Hankel function of the second kind. If we were to assume a time dependence of $e^{-j\omega t}$, then we would instead use a spherical Hankel function of the first kind. After Equation (3), we drop the Hankel function's (2) superscript.

$$P_1 = \sum_{t_1=0}^{\infty} \sum_{s_1=-t_1}^{t_1} A_{t_1 s_1}^{1}\, h_{t_1}^{(2)}(kr_1)\,\Omega_{t_1}^{s_1}(\theta_1, \phi_1)$$
$$P_2 = \sum_{t_2=0}^{\infty} \sum_{s_2=-t_2}^{t_2} A_{t_2 s_2}^{2}\, h_{t_2}^{(2)}(kr_2)\,\Omega_{t_2}^{s_2}(\theta_2, \phi_2) \qquad (3)$$

Given the Addition Theorem, we can express the pressure from sphere two relative to sphere one (see Equation (4), Ref. 7). The appendix within Ref. 7 provides the definition for the function $a(v,p,t,\mu,s)$. The angles θ_{12} and ϕ_{12} are formed by describing the location of sphere one's center relative to sphere two's center (see Figure 1). The prime in the last summation means the index is incremented by two.

$$P_2^1 = \sum_{t_2=0}^{\infty} \sum_{s_2=-t_2}^{t_2} A_{t_2,s_2}^2 \left\{ \begin{array}{l} \sum_{v_1=0}^{\infty} \sum_{\mu_1=-v_1}^{v_1} \sum_{\substack{p_1=|t_2-v_1| \\ p_1 \geq |s_2-\mu_1|}}^{t_2+v_2}{}' a(v_1,p_1,t_2,\mu_1,s_2)\, j_{v_1}(kr_1)^* \\ h_{p_1}(kd)\, \Omega_{v_1}^{\mu_1}(\theta_1,\phi_1)\, \Omega_{p_1}^{s_2-\mu_1}(\theta_{12},\phi_{12}) \end{array} \right\} \quad (4)$$

A reapplication of the Addition Theorem provides us a mathematical expression for the pressure from sphere one relative to sphere 2 coordinates.

$$P_1^2 = \sum_{t_1=0}^{\infty} \sum_{s_1=-t_1}^{t_1} A_{t_1,s_1}^1 \left\{ \begin{array}{l} \sum_{v_2=0}^{\infty} \sum_{\mu_2=-v_2}^{v_2} \sum_{\substack{p_2=|t_1-v_2| \\ p_2 \geq |s_1-\mu_2|}}^{t_1+v_2}{}' a(v_2,p_2,t_1,\mu_2,s_1)\, j_{v_2}(kr_2)^* \\ h_{p_2}(kd)\, \Omega_{v_2}^{\mu_2}(\theta_2,\phi_2)\, \Omega_{p_2}^{s_1-\mu_2}(\theta_{21},\phi_{21}) \end{array} \right\} \quad (5)$$

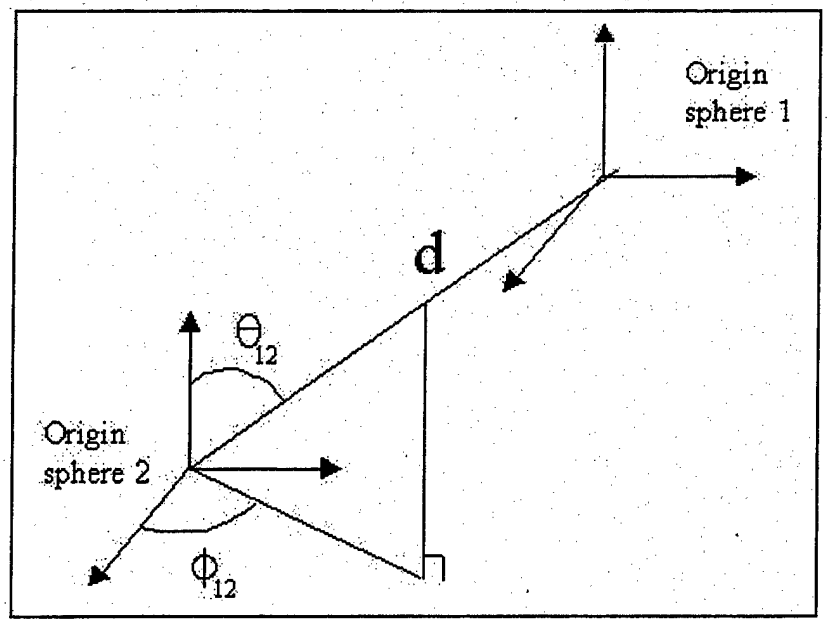

Figure 1. Orientation of sphere's origins

C. APPLICATION OF BOUNDARY CONDITIONS

Recalling the boundary condition for the sphere's surface velocity as stated in Equation (1) we obtain

$$V_1 = \frac{j}{\omega\rho_o}\frac{\partial}{\partial r}\left[P_1 + P_2^1\right]\Big|_{r_1=a} \quad \text{and} \quad V_2 = \frac{j}{\omega\rho_o}\frac{\partial}{\partial r}\left[P_2 + P_1^2\right]\Big|_{r_2=a} \qquad (6)$$

After the application of the boundary conditions, we use normal mode analysis (orthogonality) to eliminate some terms. In Equation (3) we note that the non-zero terms are those for which $t_1 = n_1$, $s_1 = m_1$, $t_2 = n_2$, and $s_2 = m_2$. Similarly, in Equations (4) and (5) the non-zero terms are

those where $\upsilon_1 = n_1$, $\mu_1 = m_1$, $\upsilon_2 = n_2$, and $\mu_2 = m_2$. Then by using the relationship with sound speed, angular frequency, and wave number ($c = \omega/k$) and dividing by a common term we obtain

$$\frac{-i\rho_o c V^{m_1}_{n_1}}{h'_{n_1}(ka)} = A^1_{n_1,m_1}\delta_{nn_1}\delta_{mm_1} + \left(\sum_{t_2=0}^{\infty} \sum_{s_2=-t_2}^{t_2} A^2_{t_2 s_2} \frac{j'_{n_1}(ka)}{h'_{n_1}(ka)} \sum_{\substack{p_1=|t_2-n_1| \\ p_1\geq|s_2-m_1|}}^{t_2+n_1}{}' a(n_1,p_1,t_2,m_1,s_2)* h_{p_1}(kd)\Omega^{s_2-m_1}_{p_1}(\theta_{12},\phi_{12}) \right) \quad (7).$$

$$\frac{-i\rho_o c V^{m_2}_{n_2}}{h'_{n_2}(ka)} = A^2_{n_2,m_2}\delta_{nn_2}\delta_{mm_2} + \left(\sum_{t_1=0}^{\infty} \sum_{s_1=-t_1}^{t_1} A^1_{t_1 s_1} \frac{j'_{n_2}(ka)}{h'_{n_2}(ka)} \sum_{\substack{p_2=|t_1-n_2| \\ p_2\geq|s_1-m_2|}}^{t_1+n_2}{}' a(n_2,p_2,t_1,m_2,s_1)* h_{p_2}(kd)\Omega^{s_1-m_2}_{p_2}(\pi-\theta_{12},\pi+\phi_{12}) \right) \quad (8).$$

Note that the first summation in each of these last two equations involves infinity. For computational purposes we must truncate to some finite number (K). Note that when K=0 the sphere is vibrating in the monopole mode. For K=1

dipole modes are kept, and when K=2, quadrupole modes are present, and so on to higher modes.

D. SOLVING FOR THE AMPLITUDE COEFFICIENTS

We can write these last two equations in a matrix form by first constructing a large column vector whose components are the stacked amplitude coefficients for spheres one and two. The ordering of the coefficients for the spheres are provided below, where $\mathbf{A}^1 = [A_{00}\ A_{1\text{-}1}\ A_{10}\ A_{11}\ \ldots.]^T$ is the vector of coefficients for sphere one.

$$\begin{bmatrix} I & B^1 \\ B^2 & I \end{bmatrix} \begin{bmatrix} \vec{A} \end{bmatrix} = \begin{bmatrix} \vec{C}^1 \\ \vec{C}^2 \end{bmatrix} \quad where \quad \vec{A} = \begin{bmatrix} A^1 \\ A^2 \end{bmatrix} \qquad (9)$$

The C vectors above each consist of one non-zero term as represented by the left-hand side of Equations (7) and (8). It can be shown that the terms of the B^1 and B^2 matrices are of order $(ka)^3$ for small ka values. This means that we can solve for the A-coefficients because we can approximate the inverse of the first large matrix of Equation (9). By the following development for small ka we can evaluate the coefficients. We drop terms on the order of ka to the sixth power.

$$\begin{bmatrix} I & B^1 \\ B^2 & I \end{bmatrix}^{-1} \approx \begin{bmatrix} I & -B^1 \\ -B^2 & I \end{bmatrix} + O(ka^6)$$

which leads to

$$\vec{A}^1 \approx \vec{C}^1 - B^1\vec{C}^2; \vec{A}^2 \approx \vec{C}^2 - B^2\vec{C}^1 \qquad (10)$$

Rewriting this approximation, shown below in Equation (11), we then have an explicit representation for the *A*-coefficients for any mode of sphere one. We can write a similar equation for sphere two. Note that the first term is due to its own mode of vibration; the next term is due to sphere two's monopole mode; the next three terms are due to sphere two's dipole modes; and the final five terms are due to sphere two's quadrupole modes. The Kronecker delta symbol (δ) equals one when the n and m values equal the value of the second subscript (i.e. first term exists when $n = n_1$ and $m = m_1$). In Equation (11), I have dropped the terms on the order of (ka) to the sixth power.

$$A^{1}_{nm} \approx \frac{-i\rho_o c V^{m_1}_{n_1}}{h'_{n_1}(ka)}\delta_{nn_1}\delta_{mm_1} + \frac{-i\rho_o c V^{m_2}_{n_2}}{h'_{n_2}(ka)} *$$

$$\left\{ \begin{array}{l} \\ \dfrac{j'_0(ka)}{h'_0(ka)} a(0,n_2,n_2,0,m_2) h_{n_2}(kd)\delta_{n0}\delta_{m0}\Omega^{m_2}_{n_2}(\theta_{12},\phi_{12}) \\ + \dfrac{j'_1(ka)}{h'_1(ka)} \quad * \\ \left[\sum_{q=-1}^{1} \sum_{\substack{p_1=\lvert n_2-1\rvert \\ p_1\geq\lvert m_2-1\rvert}}^{n_2+1}{}' a(1,p_1,n_2,q,m_2) h_{p_1}(kd)\Omega^{m_2+1}_{p_1}(\theta_{12},\phi_{12})\delta_{n1}\delta_{mq} \right] \\ + \dfrac{j'_2(ka)}{h'_2(ka)} \quad * \\ \left[\sum_{q=-2}^{2} \sum_{\substack{p_1=\lvert n_2-2\rvert \\ p_1\geq\lvert m_2-2\rvert}}^{n_2+2}{}' a(2,p_1,n_2,q,m_2) h_{p_1}(kd)\Omega^{m_2+2}_{p_1}(\theta_{12},\phi_{12})\delta_{n2}\delta_{mq} \right] \end{array} \right\} \quad (11)$$

E. SELF AND MUTUAL RADIATION IMPEDANCE

The approximation for the amplitude coefficients, Equation (11), plays an important part of my derivation of the radiation impedance. We will also make use of a relationship developed by New and Eisler (Ref. 8). Radiation impedance is defined as the ratio of force exerted by the radiator on the median to the velocity of the radiator. If the velocity of the radiator is spatially independent, the calculation is straightforward. However, when the velocity does have some spatial dependence then we must use the equation (* means complex conjugate)

$$Z_{rj} = \frac{1}{V_j V_j^*} \iint_{\substack{surface \\ of\ the \\ sphere}} p(\vec{r}_j) v_j^*(\vec{r}_j) d S_j \quad where \quad v_j = V_j \beta(\vec{r}_j) \qquad (12).$$

In applying Equation (12), note that the two identical spheres may be radiating in two distinct modes. Using Equation (12) to determine the radiation impedance for sphere one in the presence of sphere two and omitting terms on the order of $(ka)^6$ we obtain

$$\left(Z_{rs}\right)_{n_1 m_1}^{\text{mode}} \approx \frac{\iint_{S_1} \left\| \Omega_{n_1}^{m_1}(\theta_1, \phi_1) \right\|^2 d S_1}{V_{n_1}^{m_1}} *$$

$$\left\{ A_{n_1 m_1}^1 h_{n_1}(ka) + \sum_{t_2=0}^{\infty} \sum_{s_2=-t_2}^{t_2} A_{t_2 s_2}^2 j_{n_1}(ka) \sum_{\substack{p_1 = |t_2 - n_1| \\ p_1 \geq |s_2 - m_1|}}^{t_2+n_1}{}' a(n_1, p_1, t_2, m_1, s_2) * h_{p_1}(kd) \Omega_{p_1}^{s_2 - m_1}(\theta_{12}, \phi_{12}) \right\} \qquad (13).$$

Reference 9 provides an expression for the surface integral of the associated Legendre polynomials given in Equation (13). Using this expression and recalling the correct representation for dS in spherical coordinates, we obtain a general form for this surface integral

$$\iint \left\|\Omega_n^m(\theta,\phi)\right\|^2 dS = 2\pi a^2\left(n+\frac{1}{2}\right)^{-1}\frac{(n+m)!}{(n-m)!} \qquad (14).$$

We can evaluate Equation (13) for several different combinations of modes (e.g. monopole-monopole, dipole-monopole, etc…) and determine the total radiation impedance for one sphere due to both spheres. New and Eisler represent the total radiation impedance of the first sphere into the form $Z_{r1} = Z_{11} + Z_{12} * V_2/V_1$, where Z_{11} is the self-radiation impedance and Z_{12} is the mutual radiation impedance. For the monopole to monopole case we obtain the following expression for the mutual radiation impedance.

$$Z_{12} = -\rho_0 c 4\pi a^2 \frac{h_0(kd)}{\left[(ka)h'_0(ka)\right]^2} + O(ka^5) \qquad (15)$$

Upon evaluating several combinations of modes and examining the calculated mutual radiation impedance I was able to determine an approximate form for the mutual radiation impedance. For two identical spheres each

radiating in a single mode of vibration the mutual radiation impedance is written as (I omit terms on the order of $(ka)^5$)

$$Z_{12} \approx -2\pi a^2 \frac{\left(n_1+\frac{1}{2}\right)^{-1}(n_1+m_1)!\rho_0 c}{(n_1-m_1)!h'_{n_1}(ka)\,h'_{n_2}(ka)*(ka)^2} \; * \;$$

$$\sum_{\substack{p=|n_2-n_1| \\ p\geq|m_2-m_1|}}^{n_2+n_1}{}' a(n_1,p_1,n_2,m_1,m_2)\,h_p(kd)\,\Omega_p^{m_2-m_1}(\theta_{12},\phi_{12}) \qquad (16).$$

Similarly the general form for the self-radiation impedance for our sphere radiating in a general mode can be derived. Equation (17) below provides the general mode self-radiation impedance (I omit terms on the order of $(ka)^5$).

$$Z_{11} \approx \frac{-2\pi a^2 i\rho_o c}{\left(n_1+\frac{1}{2}\right)} \frac{(n_1+m_1)!}{(n_1-m_1)!} \frac{h_{n_1}(ka)}{h'_{n_1}(ka)} \qquad (17)$$

These two expressions provide a quick approximation for the mutual and self radiation impedances between two spheres each radiating in some general mode. I will hereafter refer to the mutual and self impedances calculated using Equation (16) and (17) as the "Modal Pritchard" approximation. Note that the mutual radiation impedance expression considers orientation between the two spheres. The following chapter

will investigate the utility of the mutual radiation impedance approximation, Equation (16).

III. UTILITY OF THE MODAL PRITCHARD APPROXIMATION

This chapter will investigate the utility of the Modal Pritchard Approximation for two types of problems. The first problem involves looking at the interaction between two identical spheres. Three cases of two-body problems are studied: monopoles, dipoles, and quadrupoles. The second type of problem involves one specific three-body where we find a limitation of our Modal Pritchard approximation due to its inability to handle scattering. Throughout this chapter I will use a *ka* value equal to one.

A. MUTUAL RADIATION IMPEDANCE

1. Monopole to Monopole Case

There are an infinite number of combinations of mode-mode interactions to consider, even for the case of two identical spheres. For example, considering only up to the quadrupole radiating modes we have 9x9=81 combinations of modes between two radiating spheres to examine. I will limit the following analysis to just three specific cases.

The first case will be an examination of the mutual radiation impedance between two spheres radiating as monopoles, also known as the "breathing mode". The result obtained using the "Modal Pritchard" approximation will be compared to what I will call the "Simple Pritchard" approximation. Named after R.L. Pritchard, the Simple

Pritchard approximation was developed to provide an expression for the mutual radiation impedance for two cylindrical sources placed on an infinite baffle, and was further simplified by assuming a small *ka* value (Ref. 10).

$$Z_{12} = -\mathrm{Real}(Z_{11})\, i \frac{e^{-ikd}}{kd} \quad \text{(Simple Pritchard approximation)} \qquad (18)$$

Here Z_{12} is the mutual radiation impedance between elements 1 and 2, and Z_{11} is the self radiation impedance of element 1. Despite the fact that this approximation was made for cylindrical piston sources on a theoretical infinite baffle, other researchers have used Pritchard's approximation for study of other shaped sources (Ref. 8). In doing so, the self radiation impedance is taken to be the free-field value. For the three-dimensional case, Equation (18) can be written using the spherical Hankel function as

$$Z_{12} = \mathrm{Real}[Z_{11}] * h_0(kd) \qquad (19).$$

I will compare our Modal Pritchard approximation with the Simple Pritchard approximation and note the differences. In applying Equation (19) or Equation (18), I calculated the self-radiation impedance by considering a sphere in free field environment.

To gauge the quality of the Modal and Simple Pritchard approximations, I have chosen to compare the results of these methods against a strict application of the Addition

Theorem. Please see Appendix A for the description of my application of the Addition Theorem along with the computer codes used to generate my results. I choose to use MATLAB for my calculations because of the user-friendly nature of this engineering tool. I validated my Addition Theorem results with Fortran codes written by Professor Scandrett of the Naval Postgraduate School. Professor Scandrett has continually improved his code over the last eight years, using it for several research efforts (Ref. 11).

Noting the appearance of infinity in Equations (4) and (5), we are required to truncate to some finite value for practical calculations. Mutual radiation impedance calculations using the "Addition Theorem" method have truncated this value to six. Even with this value, the computer code must solve a large (98 by 98) matrix of equations.

Figure (2) shows the calculated real part of the mutual radiation impedance (resistance) between two monopole radiating spheres. Similarly, Figure (3) shows the imaginary part (reactance). Note first of all that the x-axis of each plot is the ratio of the center-to-center distance between the spheres to the radius of the two (identical) spheres. Additionally, the impedance values have been scaled by $4\pi a^2 \rho c$.

For both the resistance and reactance parts of the impedance we observe that the results of the Modal Pritchard approximation are in excellent agreement with results of the Addition Theorem method throughout the plot ranges. The results for the Simple Pritchard approximation do not agree with the Addition Theorem results, especially at smaller values of (d/a), which corresponds to closely-spaced transducers. An analysis of the errors between the Modal Pritchard results and the Addition Theorem results, and between the Simple Pritchard results and the Addition Theorem results, was conducted. Figure (4) shows the results of this analysis. For ka = 1, the Simple Pritchard approximation breaks down when the ratio between the center to center distance and the radius is below 7.5.

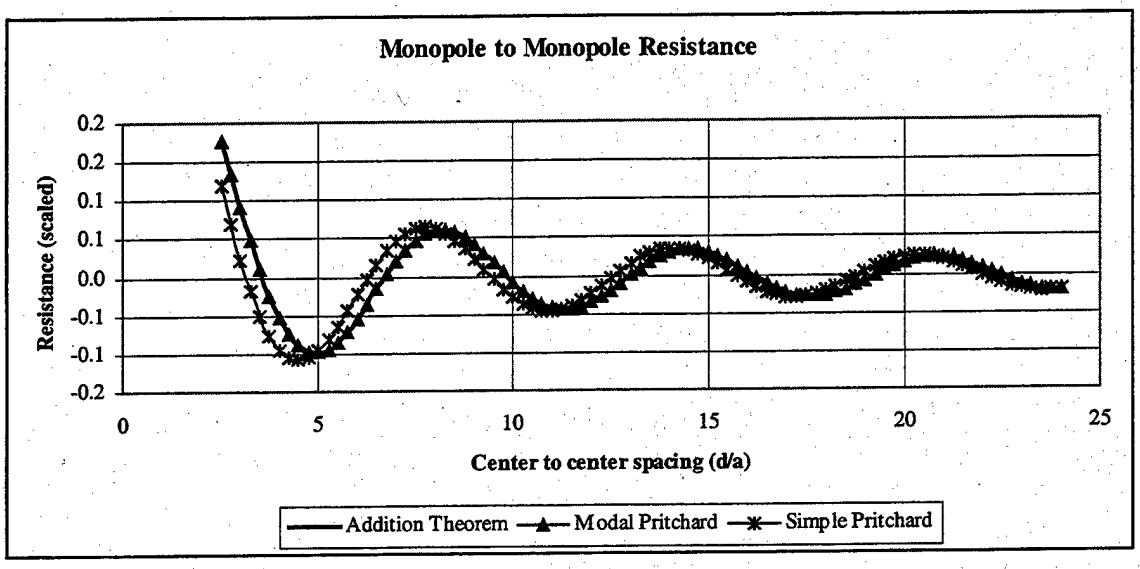

Figure 2. Monopole to Monopole Resistance

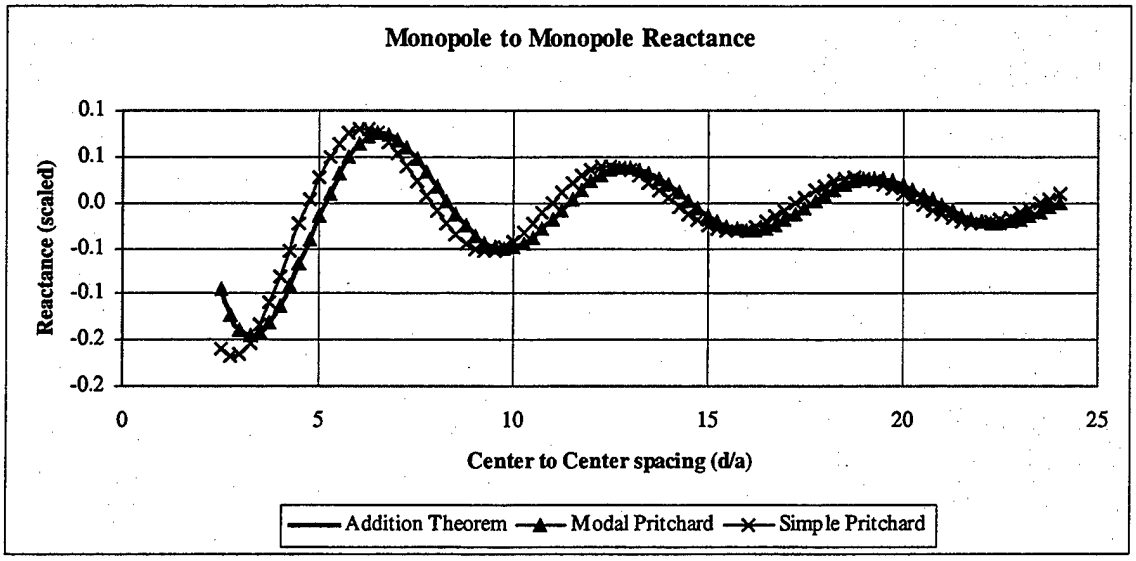

Figure 3. Monopole to monopole reactance

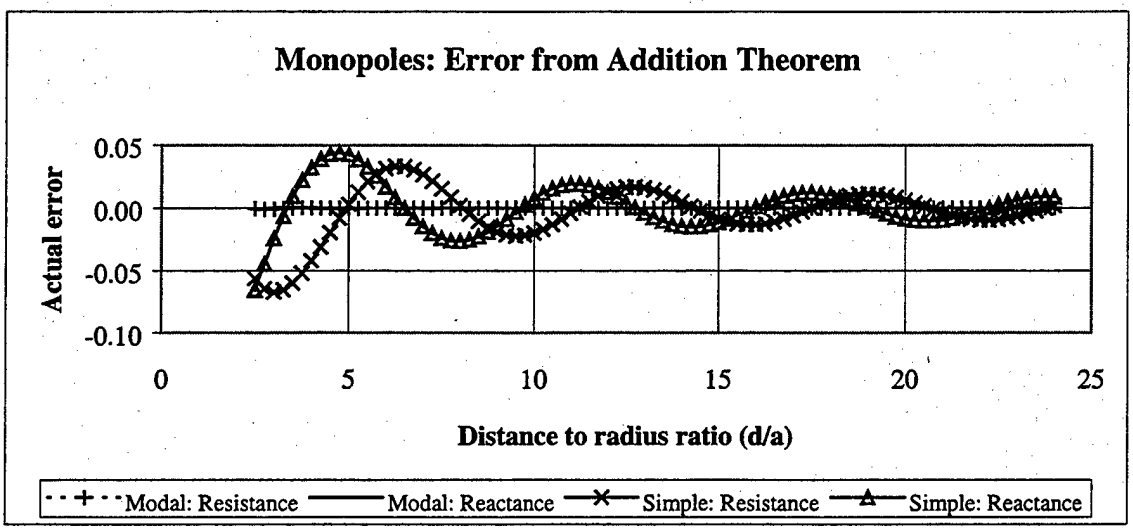

Figure (4). Monopoles, Error from the Addition Theorem

2. Dipole to Dipole Case

I conducted an analysis of the dipole-to-dipole mutual radiation impedance, similar to the above analysis I took the axes of the dipoles to be oriented along the axis joining the sphere centers. In terms of multipolar

components, this corresponds to the n=1, m=0 mode for each sphere. For the Simple Pritchard calculation I first multiplied the real part of the free-field self-radiation impedance for the hard sphere (oscillating in a dipole mode) with the appropriate Hankel function, as represented in Equation (19). This result was then multiplied by three. The reason for this correction factor is that the conventional Simple Pritchard approximation (Equation (19)) does not account for any angular orientation of the two spheres. The factor of three correction was derived by comparing the Simple Pritchard Equation (19) with the full Addition Theorem, in a small ka limit, for the dipole configuration examined (Ref. 12). For this particular analysis, I am only considering one combination (n_1=1, m_1=0, n_2=1, and m_2=0). There are a total of nine (3x3) different combinations of dipole to dipole radiation cases.

Figures (5) and (6) show the real and imaginary parts of the mutual radiation impedance for this dipole-to-dipole case. Again, note the good agreement of the Modal Pritchard results with the Addition Theorem results. Notice how the errors for the Simple Pritchard approximation increase as the ratio of sphere's spacing to the radius decreases. Figure (7) shows the errors between the results for both the Modal and Simple Pritchard approximations as compared to the results for the Spherical Addition Theorem. While the

errors for the Simple Pritchard approximation are not too bad for large values of *d/a*, they become significant when *d/a* is less than 8.0, for *ka* = 1.

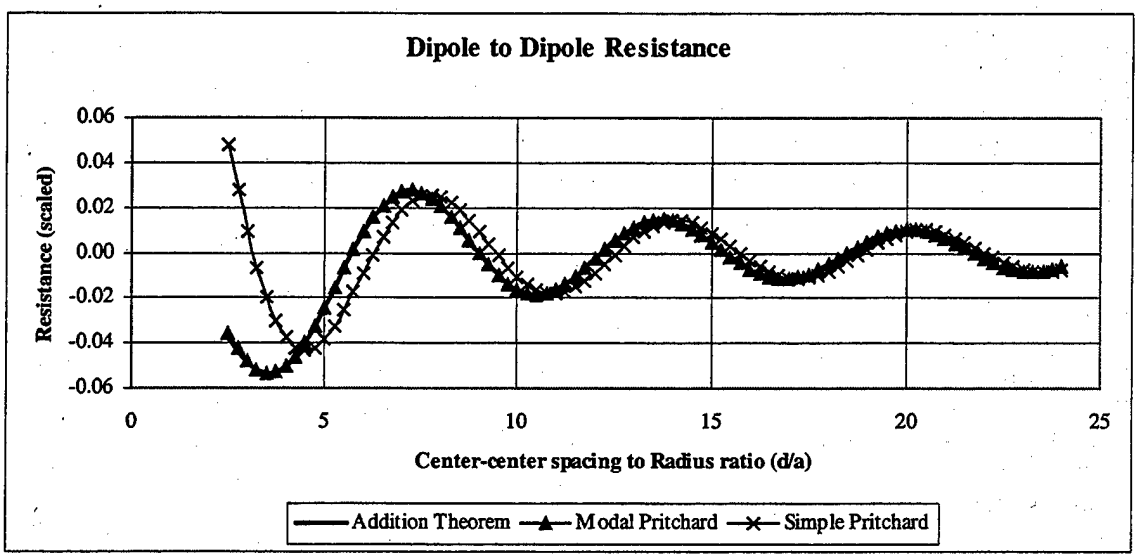

Figure 5. Dipole to dipole resistance.

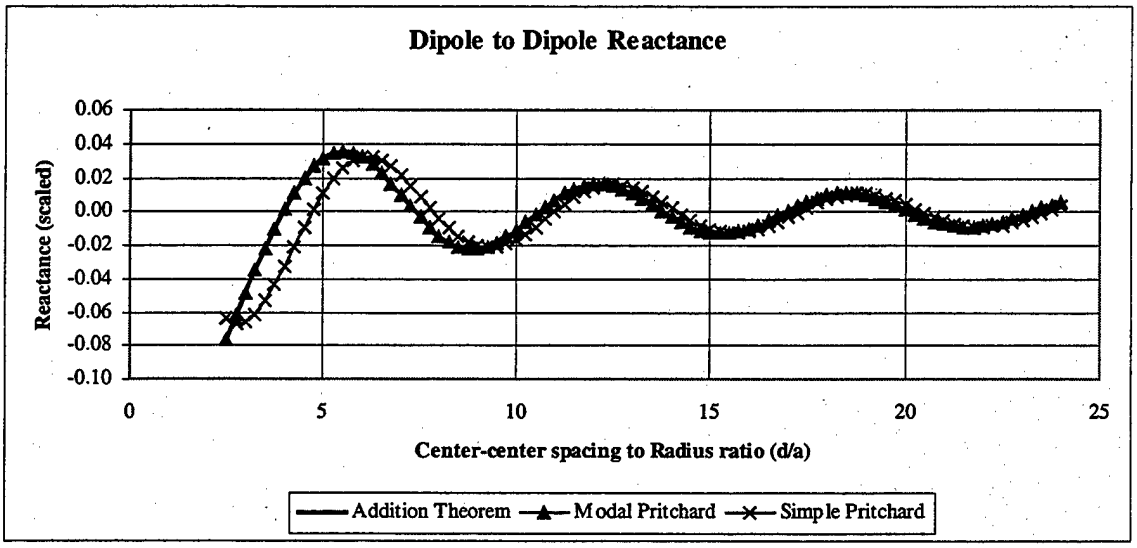

Figure 6. Dipole to dipole reactance

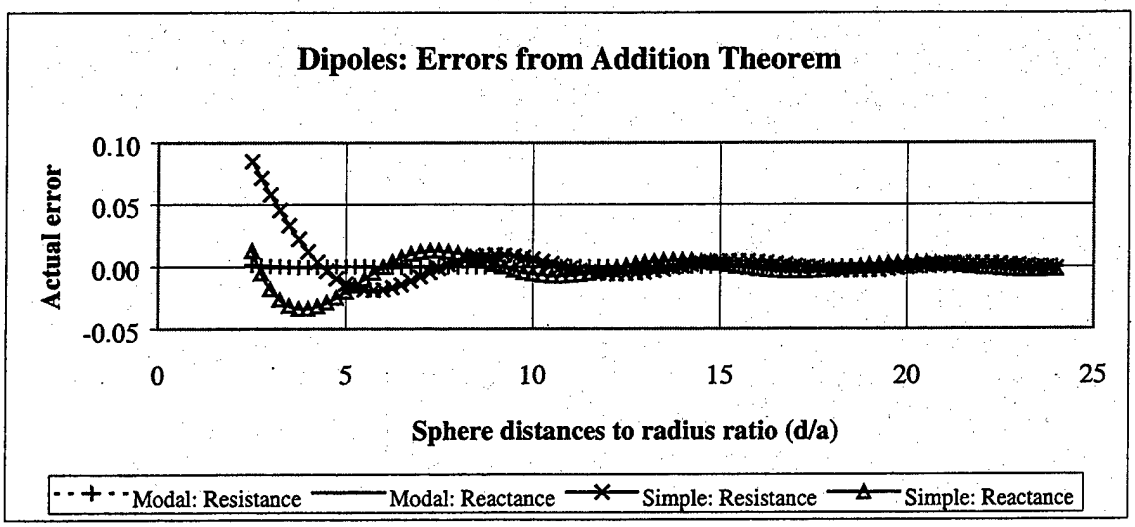

Figure (7). Dipoles, Error from the Addition Theorem

3. Quadrupole to Quadrupole Case

As a final example, I conducted an analysis of the quadrupole-to-quadrupole mutual radiation impedance. Two linear quadrupoles (n=2, m=0) were considered, with their axes aligned with the axis joining the sphere centers. For the simple Pritchard calculation I first multiplied the real part of the free-field self-radiation impedance for the hard sphere with the appropriate Hankel function, again using Equation (19). In this case, however, it can be shown that Equation (19) needs to be multiplied by a correction factor of five. Again, the reason for this correction factor, as in the dipole case, is that the Simple Pritchard formula does not account for any angular orientation of the two spheres. For this particular analysis, I am only considering one combination (n_1=2, m_1=0, n_2=2, and m_2=0).

There are a total of twenty-five different combinations of quadrupole to quadrupole radiation.

Figures (8) and (9) show the real and imaginary parts of the mutual radiation impedance for this quadrupole-to-quadrupole case. We continue to note the good agreement of the Modal Pritchard results with the Addition Theorem results. Notice again how the error in the Simple Pritchard results increases as the ratio between the sphere spacing and sphere radius decreases. Figure (10) shows the errors between both the Modal and Simple Pritchard results as compared to the results using the Spherical Addition Theorem. While the errors for the Simple Pritchard approximation are not too bad at large values of d/a, they become significant when d/a is less than 8.0, for $ka = 1$. This continues to show how the Simple Pritchard approximation breaks down as the transducers' spacing decreases.

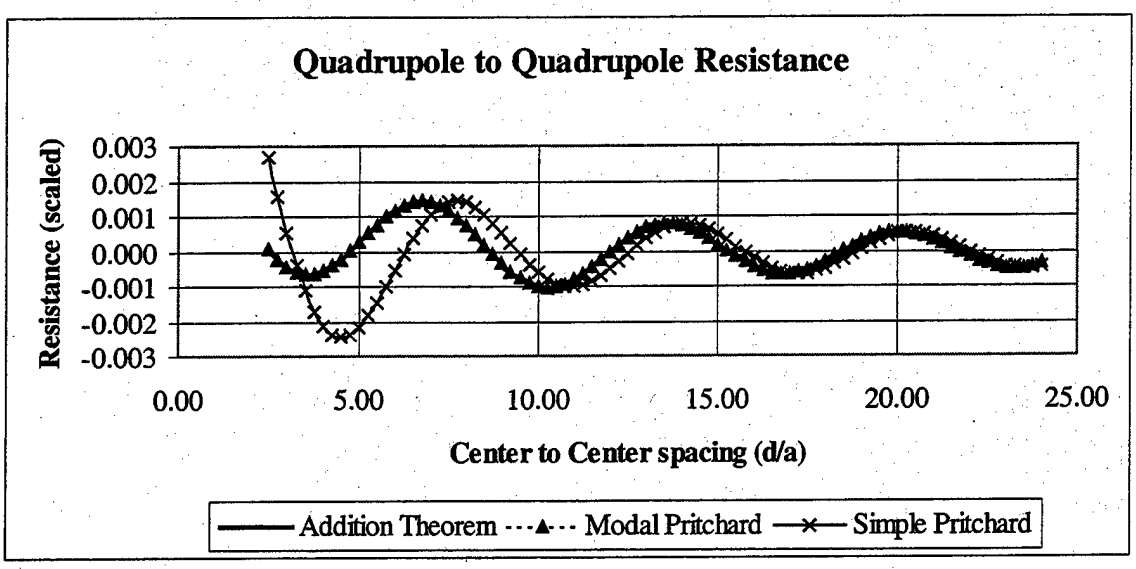

Figure (8). Quadrupole to Quadrupole Resistance

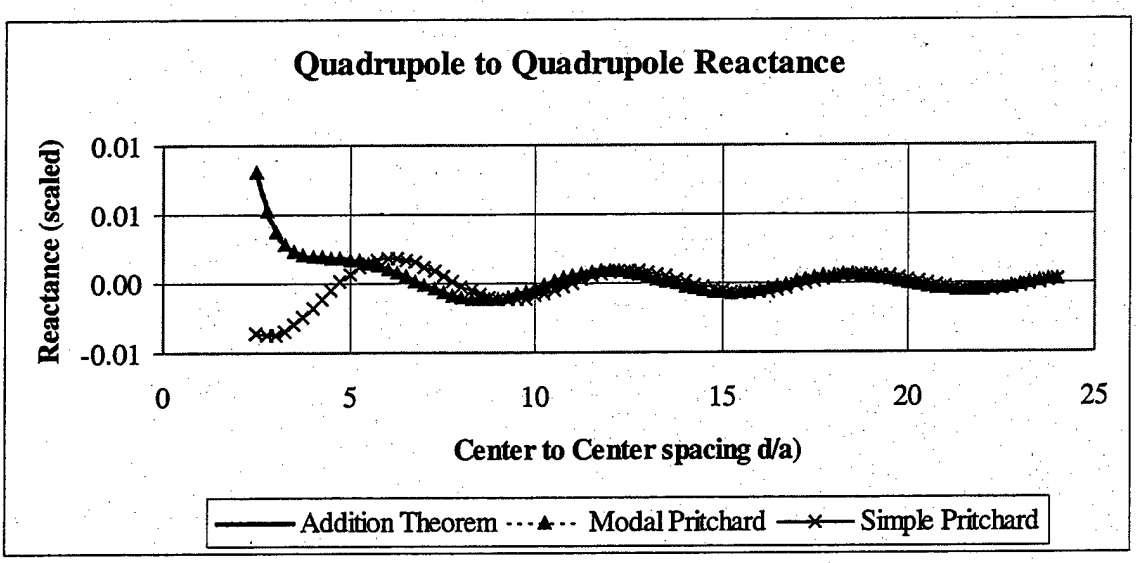

Figure (9). Quadrupole to Quadrupole Reactance

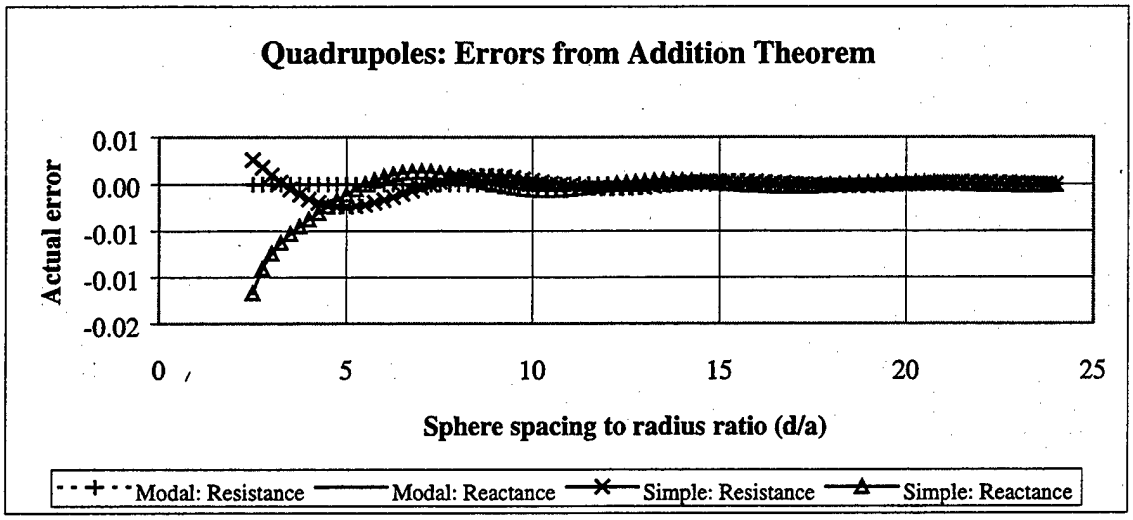

Figure (10). Quadrupoles, Errors from Addition Theorem

B. EXAMINATION WITH THREE A BODY PROBLEM

To further examine our Modal Pritchard approximation for the mutual radiation impedance, we considered the following three-body problem (see Figure 11).

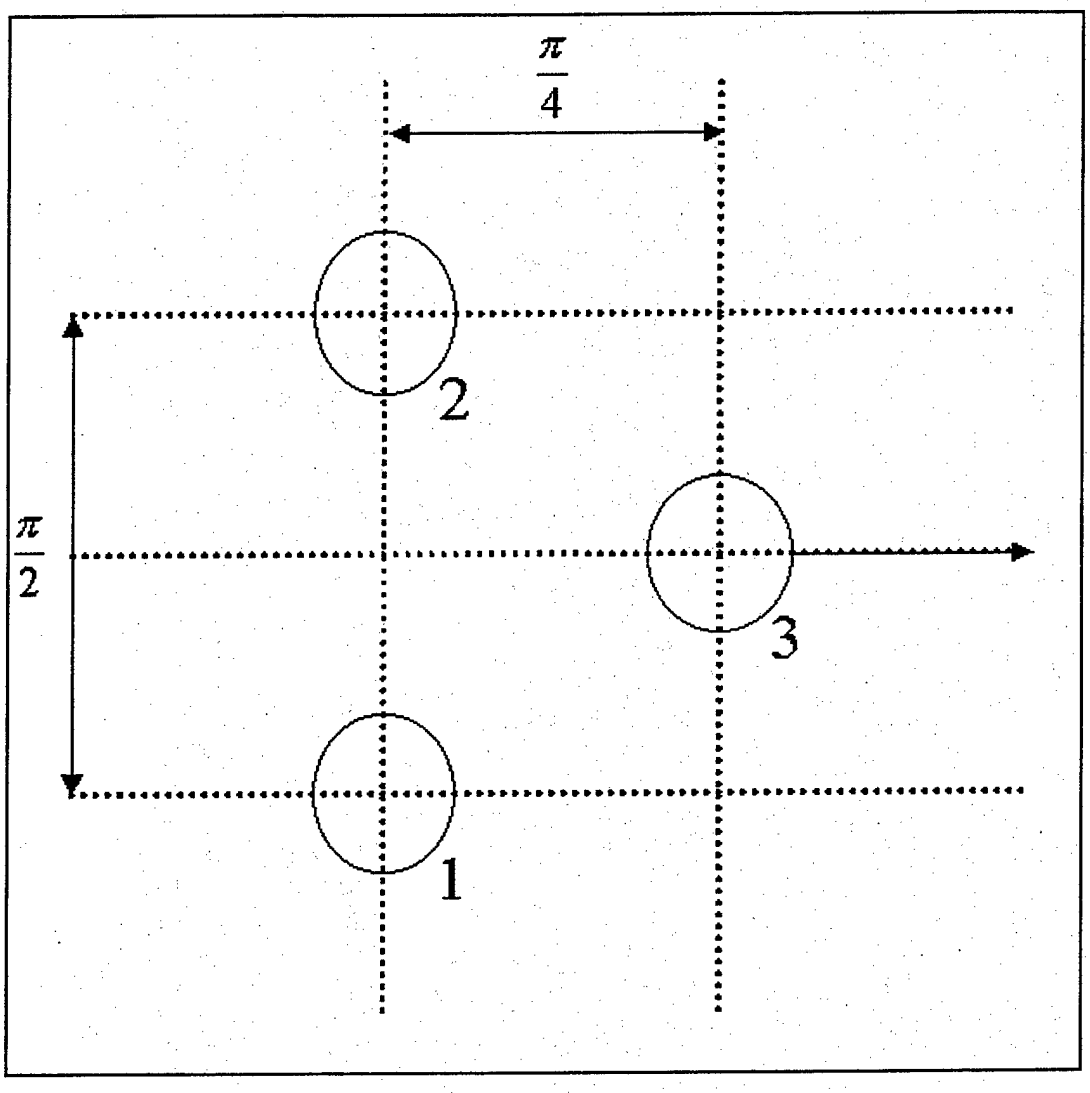

Figure (11). Drawing of a Three-Transducer Problem.

In this problem we will set spheres one and two to radiate as monopoles. These two transducers will maintain the same physical dimensions and operating characteristics as before (i.e. frequency = 474 Hz, sound speed of 1490 m/sec, radius = 0.5 m, ka = 1, therefore the wavelength equals π). Sphere three will be considered acoustically hard. We examine the mutual radiation impedance for sphere one due to the presence of all three spheres. Additionally, we will examine the effect of moving the third sphere horizontally away from the axis of the other radiating spheres. We will investigate the performance of our Modal Pritchard approximation for this three-body problem and compare these results with the results using the full Addition Theorem. As shown in Figure (11), sphere three's starting distance from the axis is one quarter of a wavelength ($D = \pi/4$).

Figure (12) shows a plot of the mutual radiation resistance, comparing the results of our modal Pritchard approximation with those of the Addition Theorem. The x-axis for this plot, as well as Figures (13) and (14), is the ratio of the distance (D) to the radius of the spheres. Additionally, the results have been scaled by $4\pi a^2 \rho c$. Figure (13) shows the reactance (or imaginary) portion of the mutual radiation impedance. Figure (14) shows the

relative error in the magnitudes of the results for the Modal Pritchard approximation against those for the full Addition Theorem. Discussions explaining my results follow Figure (14).

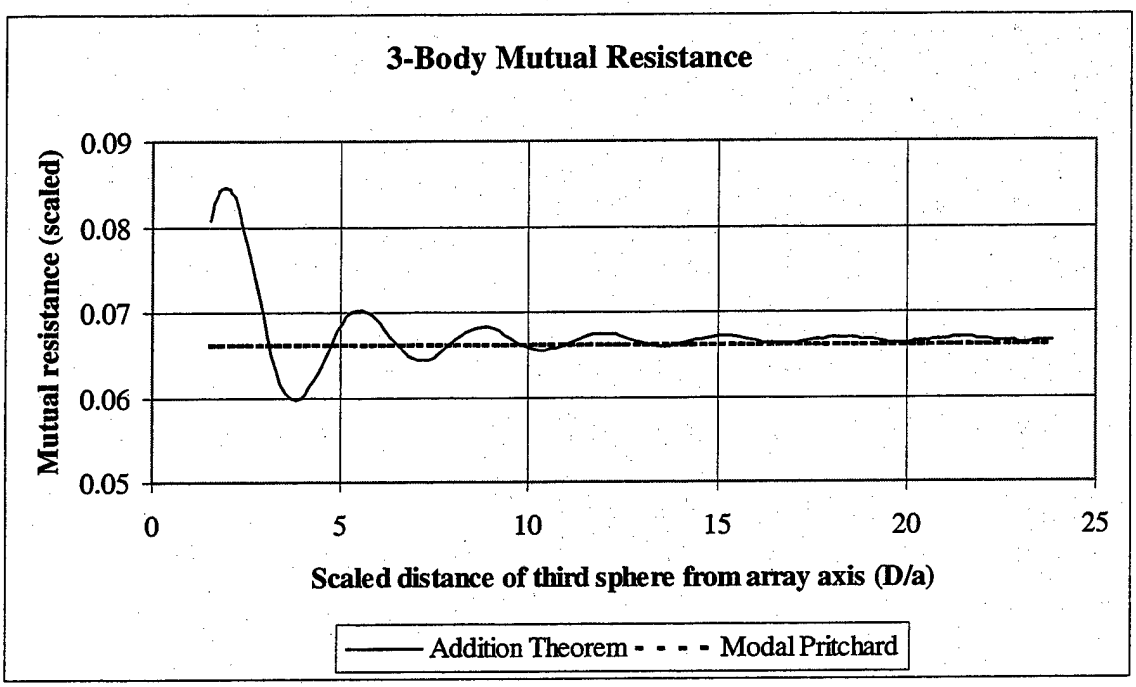

Figure (12). Mutual Resistance, Three-Body Problem

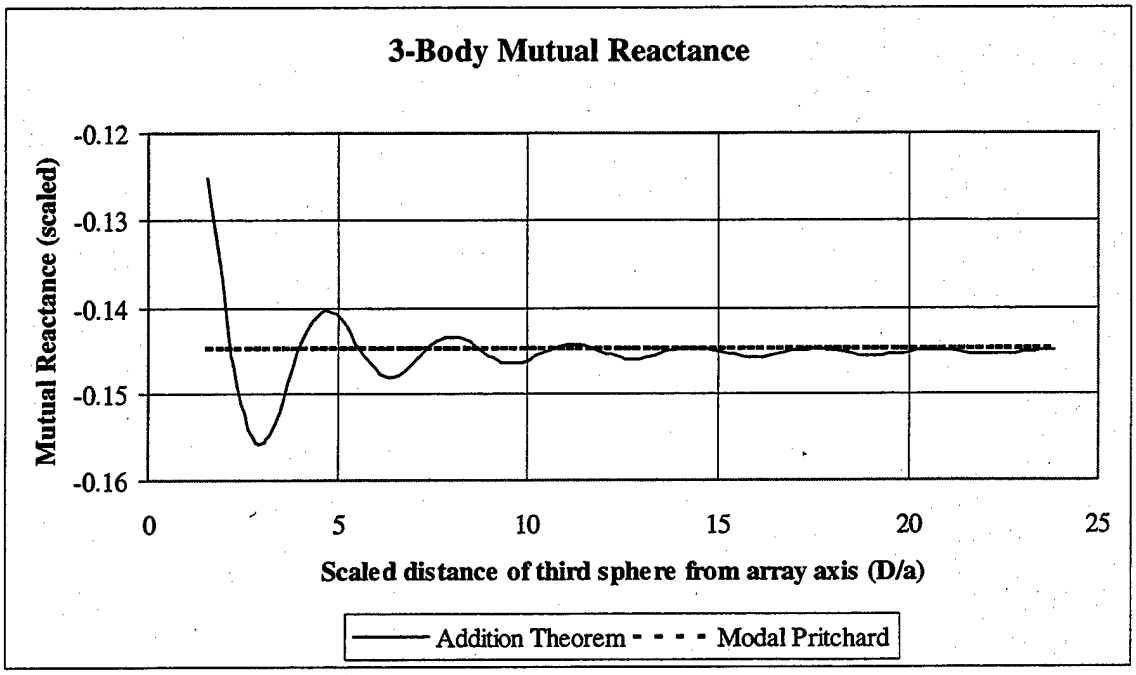

Figure (13). Mutual Reactance, Three-Body Problem

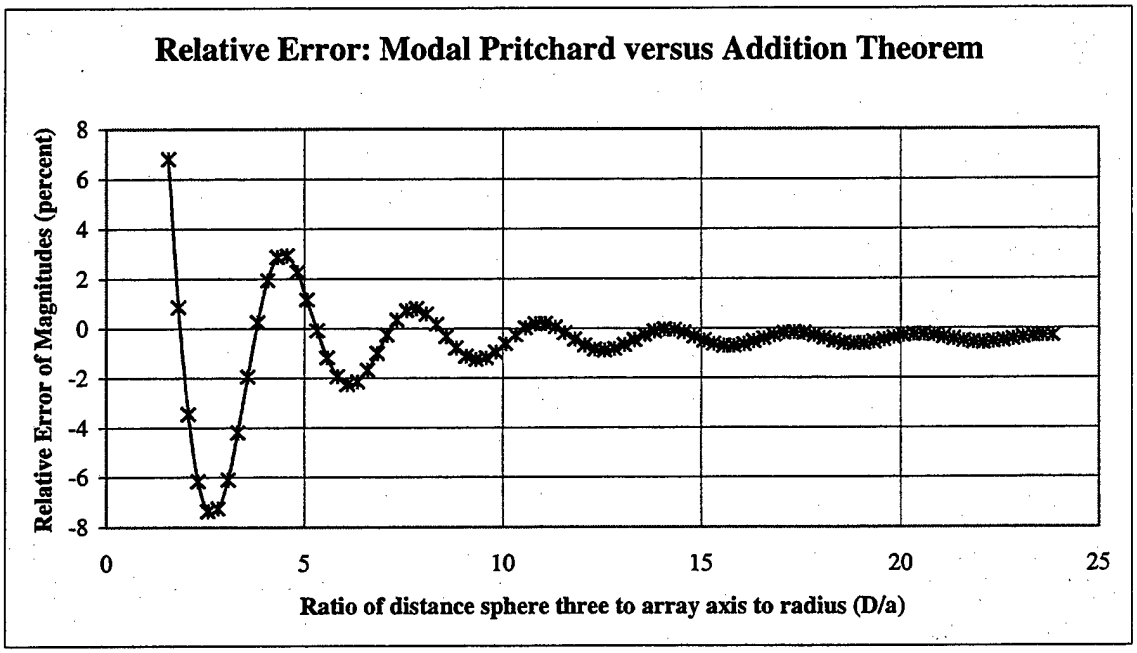

Figure (14). Relative Error, Modal Pritchard vs Addition Theorem.

The modal impedance approximation as I am using it here neglects scattering. This is why we see the straight lines for the Modal Pritchard results in Figures (12) and (13). Because the Modal Pritchard approximation does not account for the scattering, this provides an argument for using the full Addition Theorem to calculate impedance when scattering is important. Appendix B provides the method and computer code I used to calculate the Addition Theorem results for this three-body problem.

I defined the relative error, as plotted in Figure (14), as (Modal Pritchard-Addition Theorem)/Addition Theorem. Therefore, dips in Figure (14) represent occurrences when the Addition Theorem results have a larger magnitude than the magnitude of the Modal Pritchard approximation results. Conversely, peaks represent occurrences for which the Addition Theorem results are smaller in magnitude. Through the use of the Addition Theorem, one can show that these peaks and valleys result from the effect of scattering.

The data used to generate Figure (14) provides the *D/a* values where these valleys and peaks occur. The first two valleys occur at the following *D/a* values: 2.57 and 6.07. The first two peaks occur at the following *D/a* values: 4.57 and 7.82.

I propose and will sketch out how these valleys and peaks occur, due to scattering effects, by evaluating the sum of the pressure waves arriving at sphere one. I will limit this evaluation by only looking at the monopole case. Since the Addition Theorem correctly handles scattering, the Addition Theorem results provide local maximum values when the scattering waves from sphere three are in phase with the direct path waves from sphere two. Similarly, the Addition Theorem results have local minimum values when the scattering waves are 180° out of phase with the direct path's phase. Our Modal Pritchard approximation does not handle the scattering effects, note the flat plots in Figures (12) and (13) for the Modal Pritchard results.

Using the Addition Theorem and considering only the monopole case, the pressure waves are of the form of outgoing spherical Hankel function as shown below.

$$h_0^{(2)}(kr_i) = j_0(kr_i)\, h_0^{(2)}(kd_{ij}) \qquad (20)$$

An examination of the direct path wave from sphere two to sphere one and of the reflected wave from sphere two, reflected off sphere three towards sphere one, was completed by Professor Scandrett (Ref. 12). The expression for the sum of these waves at sphere one is provided below. The first term in the bracket is due to the direct path and the

second term is due to the reflected (scattered) wave. The A is some arbitrary amplitude coefficient.

$$A\, j_0(k_i a)\left\{h_0^{(2)}(kd_{12}) - \frac{j_0'(ka)}{h'(ka)}\left[h_0^{(2)}(kd_{13})\right]^2\right\} \qquad (21)$$

A plot of Equation (21) is provided in Figure (15) in terms of *D/a* versus magnitude. The peaks of Figure (15) match the valleys of Figure (14). Similarly, local minimums of Figure (15) match the peaks of Figure (14). The first two peaks of Figure (15) are at *D/a* values of 2.57 and 6.07 and the first two local minimums are at *D/a* values of 4.57 and 7.82. The maximum values occur when the scattering waves are in phase with the direct path waves. The minimum values of Equation (21) occur when the scattering wave is 180 degrees out of phase with the direct path.

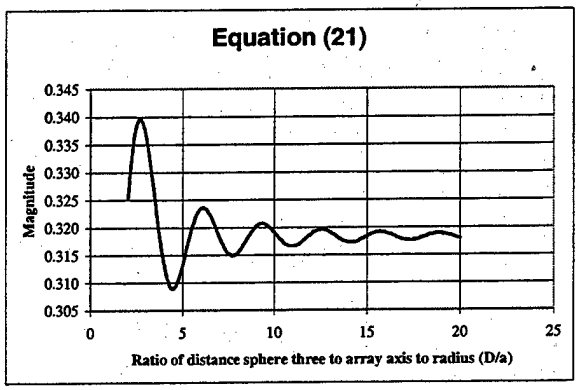

Figure (15): Plot of Equation (21)

Figure (16) provides an additional drawing of this three-body problem and shows the distance parameters (d_{12} and d_{13}) used in Equation (21).

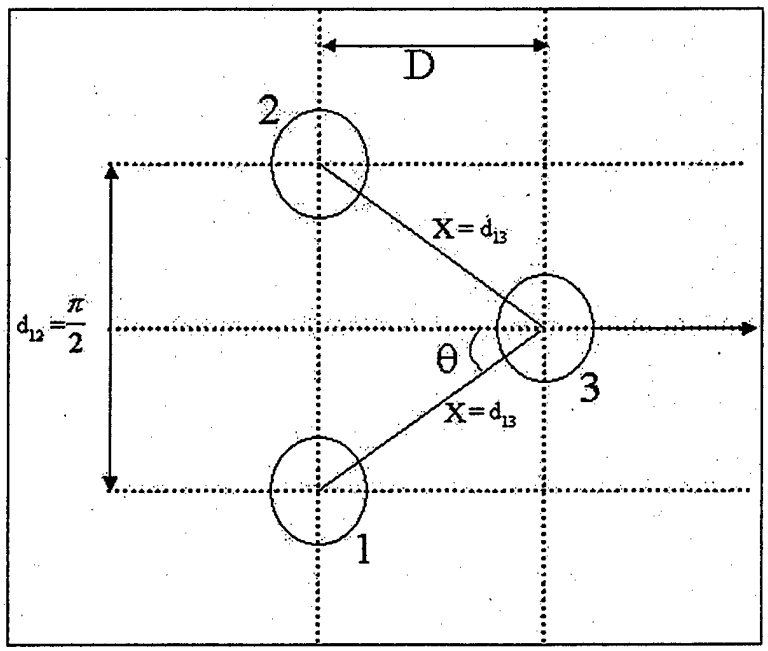

Figure (16). Three-body problem drawing two.

Again, the full Spherical Addition Theorem is recommended over our Modal Pritchard approximation when scattering is an important consideration as in this three-body problem.

(THIS PAGE INTENTIONALLY LEFT BLANK)

IV. NUMERICAL MODELING WITH ATILA

This chapter describes the ATILA finite-element model used to calculate the scattering of acoustic waves from an elastic sphere in water. The goal is to compute the so-called T-matrix, which relates the scattered waves to the incident waves, in an orthogonal (spherical harmonic) basis set (Ref. 11).

A. MODEL INTRODUCTION

A few comments about ATILA are appropriate at this time. As mentioned in the introduction, ATILA is a French designed finite element code specifically developed to model sonar transducers. ATILA, written mostly in standard FORTRAN 77, is the result of many years of research done at the Insitut Superieur d'Electronique du Nord. It is quite large, consisting of over 200,000 lines of code (Ref. 13).

This tool has been used by NPS faculty and masters thesis students for several years and has been updated at least three times. Recent studies have helped to identify needed modifications to the code, such as increasing the maximum allowable number of degrees of freedom, and modification of the numerical techniques used to handle the radiation boundaries. For example, during the calculation of the entries for the transition matrix (T-matrix) there were noted errors when compared to answers derived from a

known analytical solution to the problem (Ref. 11). The ATILA version I used (5.1.1) did increase the maximum allowable degrees of freedom, but has yet to address the radiation boundary problem.

B. ATILA AND MESH DESCRIPTION

1. About the Model

A distinguishing characteristic of ATILA is the use of isoparametric elements for both the shell elements and the fluid elements. Isoparametric elements are elements that use the same shape function for geometric mapping as well as field calculations (Ref. 4). The major advantage of isoparametric elements is that they lend themselves well to numerical integration. This is because of the nature of isoparametric elements. These elements are defined in the natural domain to be normalized, thus making numerical integration much easier to apply (Ref. 4). Also, when isoparametric elements are used, fewer nodes are needed to define the mesh than without such elements.

Other numerical techniques for solving the acoustic equations have been used by U.S. Navy labs. One method used for many years at the Naval Ocean Systems Center is called CHIEF (Combined Helmholtz Integral Equation Formulation) (Ref. 2). CHIEF, which models acoustic radiation from bodies with arbitrary shapes does not use isoparametric elements. Thus we should expect a higher degree of accuracy

with ATILA over CHIEF. One advantage to CHIEF is that the radiation boundary condition is "built-in" to the boundary element by its use of the Helmholtz Integral Equation. Currently, this provides an advantage over ATILA, which employs so-called "monopolar" and "dipolar" "dampers". These dampers can not represent a perfectly absorbing radiation boundary for a higher order multipolar field.

The basic set of equations that allow for a large number of analysis to be performed include elasticity in the structure, the Helmholtz equation in the fluid, and Poisson's equation in the elastic or piezoelectric material. Primary variables found using ATILA include the displacement field $\underline{U}$ in the whole structure, the electric potential $\underline{\Phi}$ in the piezoelectric material, and the pressure $\underline{P}$ in the fluid. In matrix form the equations are as follows (Ref. 13).

$$\begin{bmatrix} ([K_{uu}]-\omega^2[M]) & [K_{u\phi}] & -[L] \\ [K_{u\phi}] & [K_{\phi\phi}] & [0] \\ -\rho^2 c^2 \omega^2 [L]^T & [0]^T & ([H]-\omega^2[M_1]) \end{bmatrix} \begin{bmatrix} \underline{U} \\ \underline{\Phi} \\ \underline{P} \end{bmatrix} = \begin{bmatrix} \underline{F} \\ -\underline{q} \\ \rho c^2 \underline{\Psi} \end{bmatrix} \quad (22)$$

Vectors in the above equations are:

$\underline{U}$= nodal values of the components of the displacement field,

$\underline{\Phi}$= nodal values of the electric potential,

$\underline{P}$= nodal values of the pressure field,

$\underline{F}$= nodal values of the applied forces,

$\underline{q}$= nodal values of the electric charges, and

$\underline{\Psi}$= nodal values of the integrated normal derivative of the pressure on the surface boundary S.

Matrices in Equation (22) include

K_{uu} = stiffness matrix,

$K_{u\phi}$ = piezoelectric matrix,

$K_{\phi\phi}$ = dielectric matrix,

M = consistent mass matrix,

H = fluid (pseudo-) stiffness matrix,

M_1 = consistent (pseudo-) fluid mass matrix,

L = coupling matrix at the fluid structure interface, and

O = zero matrix.

In addition,

ω= Angular frequency,

ρ = Fluid density,

c = fluid sound speed, and

^{T} = means transposition of a matrix.

2. Three-dimensional Fluid Mesh

To run this and other finite element models you need to split the region under study into elements; the ATILA code has an extensive library of elements available. These elements are distinguished by a set ordering of nodes and

the node coordinates. Figures 16 provides a Mercator projection of the eight "super-elements" used for one of the several layers under study. These super elements are the start of the mesh generation. The solid lines and nodes (dots with numbers) define the super-elements. The dotted lines show how the super-elements are sub-divided. Laid out 3-dimensnionally, Figure 17 represents the super-elements that make up the spherical transducer under study, a spherical shell with a radius of 0.5 m. Using a finite element mesh generator called MOSAIQUE, I built a complex mesh of the entire field using the super-elements, using special instructions for subdividing the elements into a large number of elements and nodes that will define each layer of the field. Figure 18 provides a detailed look of the field under study (the fluid outer boundary is at 5 meters).

There are several layers that make up the entire mesh some of which are full-layers and some are mid-layers. Each full-layer consists of 194 nodes of which 18 are nodes of the super-elements. Mid-layers have a total of 62 nodes. Starting from the innermost radius and working outward, the complete three-dimensional mesh consists of the following layers. First is the shell layer that consists of 194 nodes. This is the actual spherical shell transducer that is being analyzed. Next, another 194 nodes are used to

describe the interface elements used to model the shell-to-water interface. This layer shares the same coordinate locations as the shell's nodes. Following this are ten fluid layers, the first two of which are 0.25 meter thick and the remaining are 1.0 meter thick. Each fluid layer consists of a full-layer and a mid-layer. Finally completing this three-dimensional mesh we have the radiation boundary elements. These last elements are used to prescribe monopolar-only or monopolar and dipolar radiation boundary conditions and are used to terminate the mesh.

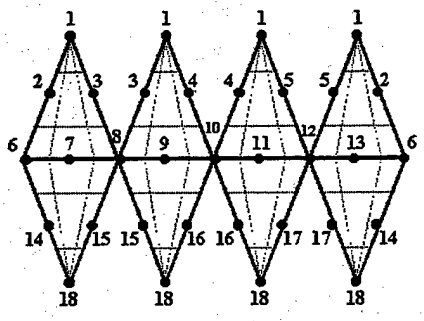

Figure 17. The Super-Element (Macerator projection)

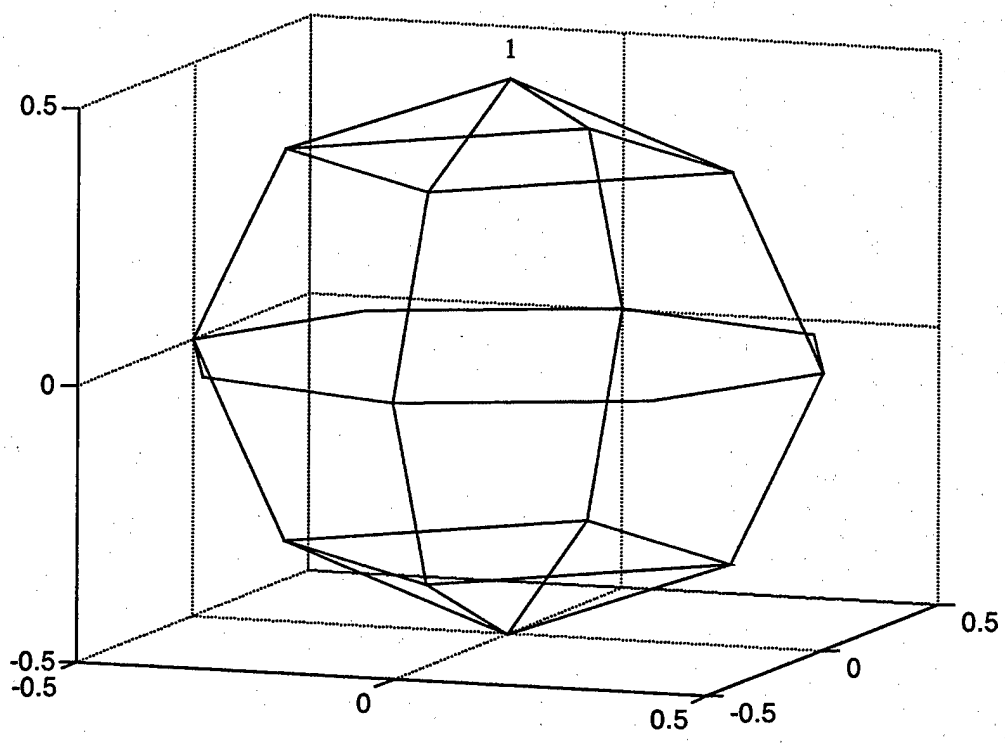

Figure 18. Super-Element (3-Dimensional view)

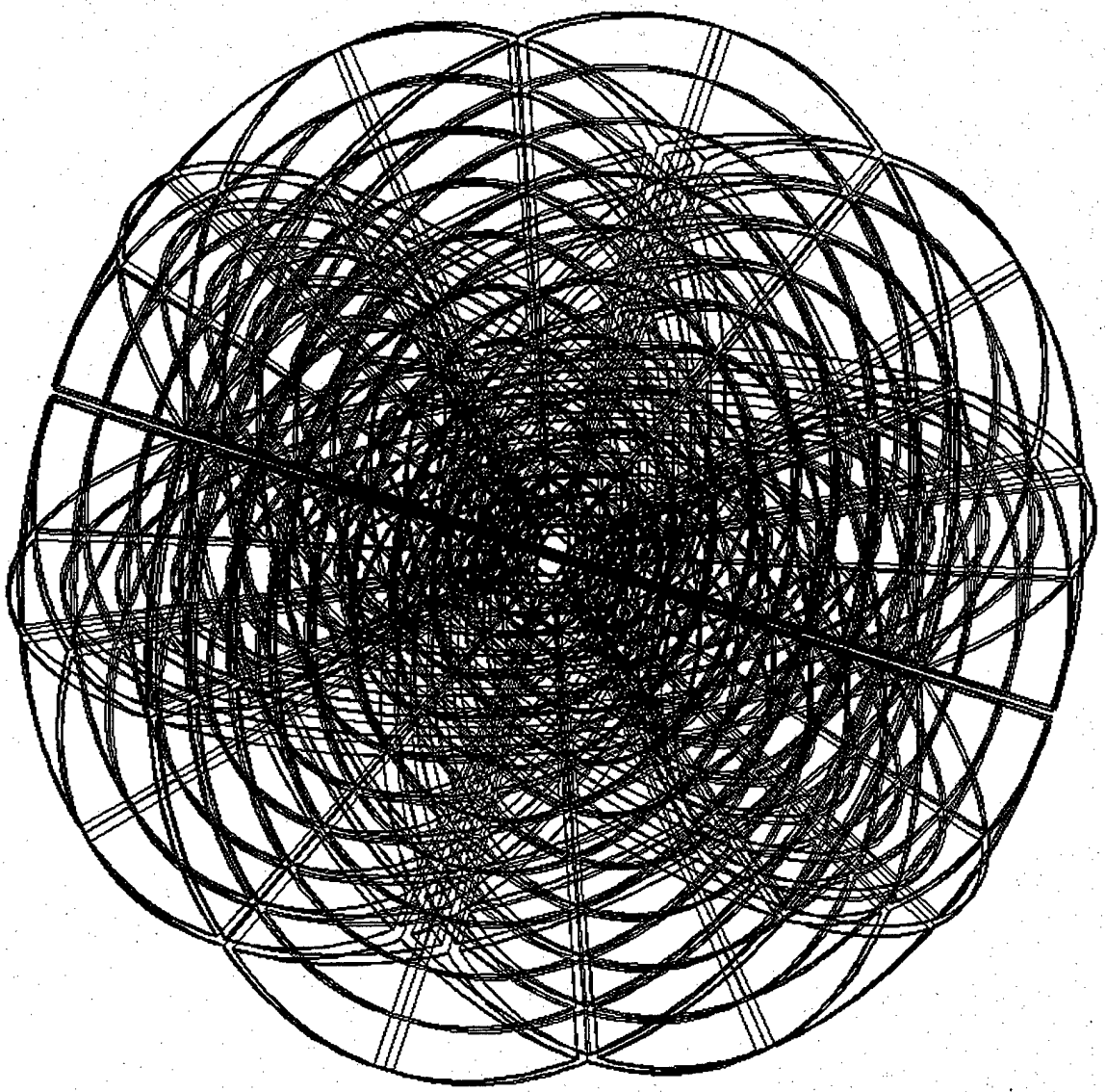

Figure 19. The complete Mesh

V. NUMBERICAL MODELING WITH ATILA: RESULTS AND DISCUSSION

A. OBJECTIVES AND THE T-MATRIX

My objectives for the numerical modeling portion of this thesis were to investigate the finite element mesh mentioned earlier, simplify the process of calculating the Transition Matrix (or T-Matrix), and provide a new method of evaluating the off-diagonal elements of the T-matrix. The finite element code is used to numerically calculate the scattered pressures from an object under study. We then use these results to calculate the object's specific T-Matrix.

In this chapter, I will document the results of the T-matrix calculation and compare with previous numerical modeling efforts. Several references mention and thoroughly discuss the definition, usage, and calculation of the T-Matrix (Ref. 3 and 5). I will simply mention here in the text that the T-Matrix describes the scattering properties of a specific body. It does this by using a discrete basis set spherical harmonics in our case, and is used to show how the incident pressure waves translate to scattered waves from the body. Please see Appendix C for more information about the T-Matrix and how I calculated the elements of the T-Matrix for our radiating body.

B. RESULTS

In order to gauge the accuracy of our T-Matrix calculation we compare our answers with an analytically derived equation. An expanded discussion of the derivation of the analytical solution can be found in a Master's Thesis by Ruiz (Ref. 5 and references therein). For a thin spherical shell the T-Matrix is diagonal, and are given by

$$R_{nm} = -\left\{\frac{i Z_n j_n'(ka) + \rho_f c_f j_n(ka)}{i Z_n h_n'(ka) + \rho_f c_f h_n(ka)}\right\} \tag{23}$$

where

$$Z_n = i\frac{h c_p \rho_s}{a\Omega}\left\{\frac{[\Omega^2 - 2(1+\nu)][\Omega^2 + 1 - \nu - \lambda_n) - \lambda_n(1+\nu)^2}{\Omega^2 + 1 + \nu - \lambda_n}\right\}$$

$$\Omega = \frac{\omega a}{c_p}, \quad c_p = \sqrt{\frac{E}{\rho_s(1-\nu^2)}} m/s, \quad \omega = 2\pi f, \quad \lambda_n = n(n+1)$$

ν = *Poisson's ratio* (0.33); h = *shell thickness* (1 *cm*)

c_p = *shell's plate velocity*

E = *Young's* mod*ulus* ($0.125x10^{12}$)

a = *spherical shell radius* (0.5 *meter*)

ρ_s = *shell's density* (7500 kg/m^3); f = *frequency* (474 *Hz*)

ρ_f *and* c_f = *fluid density* (1000 kg/m^3) *and speed* (1490 m/s).

The calculation for this analytical solution was performed using MATLAB and the computer program can be found at the end of Appendix C. In the following discussion, when

referring to errors, I am comparing the calculated values with the analytical solutions from Equation (23).

Using the thin spherical shell parameters listed above and the MATLAB computer script provided in Appendix C, I calculated the analytical T-Matrix diagonal elements (the off-diagonal elements are zero for a spherically symmetric scatter). These diagonal elements are provided in Table I below. A value of ka = 1 was used (frequency = 474 Hz).

ANALYTICAL DIAGONAL T-MATRIX ENTRIES				
ELEMENT	REAL PART	IMAGINARY PART	MAGNITUDE	PHASE (DEGREES)
$T_{11} = R_{00}$	-1.3465E-02	1.1525E-01	1.1604E-01	96.6635
$T_{22} = R_{1-1}$	-6.0255E-03	7.7390E-02	7.7624E-02	94.4520
$T_{33} = R_{10}$	-6.0255E-03	7.7390E-02	7.7624E-02	94.4520
$T_{44} = R_{11}$	-6.0255E-03	7.7390E-02	7.7624E-02	94.4520
$T_{55} = R_{2-2}$	-6.1773E-04	-2.4847E-02	2.4854E-02	-91.4242
$T_{66} = R_{2-1}$	-6.1773E-04	-2.4847E-02	2.4854E-02	-91.4242
$T_{77} = R_{20}$	-6.1773E-04	-2.4847E-02	2.4854E-02	-91.4242
$T_{88} = R_{21}$	-6.1773E-04	-2.4847E-02	2.4854E-02	-91.4242
$T_{99} = R_{22}$	-6.1773E-04	-2.4847E-02	2.4854E-02	-91.4242

Table I. Analytical Diagonal T-Matrix Entries.

I then used the finite element code (ATILA) to model the scattering pressure field generated by the thin spherical shell. With the scattered pressure results, I calculated the T-Matrix entries column by column. These results are provided below in Table II.

Numerical Diagonal T-Matrix Elements				
Element	Real Part	Imaginary Part	Magnitude	Phase (Degrees)
T_{11}	-1.6107E-02	1.2894E-01	1.2994E-01	97.1202
T_{22}	-8.0999E-03	7.9943E-02	8.0353E-02	95.7855
T_{33}	-7.7968E-03	7.9777E-02	8.0157E-02	95.5819
T_{44}	-8.0801E-03	7.9946E-02	8.0353E-02	95.7713
T_{55}	-2.1393E-03	-1.5865E-02	1.6009E-02	-97.6794
T_{66}	-2.2524E-03	-1.5923E-02	1.6082E-02	-98.0513
T_{77}	-2.1536E-03	-1.5930E-02	1.6075E-02	-97.6994
T_{88}	-2.2501E-03	-1.5925E-02	1.6084E-02	-98.0420
T_{99}	-2.1498E-03	-1.5860E-02	1.6005E-02	-97.7193

Table II. Numerical Diagonal T-Matrix Elements.

Table III, next page, provides an error analysis for the current results. Unfortunately, the monopole result (i.e. the first diagonal element) is much worse than previous results. All other diagonal elements show some improvement over previous work, between 6 and 56 percent improvement in their magnitudes. But the most important indicator is the monopole element; therefore, our new mesh does not provide a significant improvement to the T-Matrix calculation. As the ATILA code is further improved we hope that these errors will be corrected.

Error Comparison Current vs. Previous						
Element	Magnitude Error (percent)	Phase Error (Degrees)	Previous Mag. Error (percent)	Previous Phase Error (Degrees)	Magnitude Improve (percent)	Phase Improve (Degrees)
T_{11}	11.984	0.457	-0.910	-0.360	-1216.94	-0.10
T_{22}	3.515	1.333	6.490	0.329	45.84	-1.00
T_{33}	3.263	1.130	7.330	-0.500	55.48	-0.63
T_{44}	3.516	1.319	6.470	0.314	45.66	-1.01
T_{55}	-35.588	-6.255	-37.800	-9.186	5.85	2.93
T_{66}	-35.296	-6.627	-38.000	-9.006	7.12	2.38
T_{77}	-35.324	-6.275	-37.700	-7.823	6.30	1.55
T_{88}	-35.288	-6.618	-38.000	-8.986	7.14	2.37
T_{99}	-35.605	-6.295	-37.900	-9.106	6.05	2.81

Table III. Error Comparison Current vs. Previous.

The T-Matrix must be diagonal due to the symmetry of the object. That means that the off-diagonal elements must be zero. Previous work documented eight significant off-diagonal elements. Current results reveal these same eight elements are the most significant off-diagonals. However, the new results show improvement, meaning the new off-diagonal values are much closer to zero than previous calculations. Along with matching the analytical diagonal elements, making all off-diagonal elements closer to zero is another indication of how well our finite element method is working. Table IV offers a comparison of this improvement. The last column of this table shows the percentage closer to zero the new off-diagonal magnitudes are compared to the previous work.

SIGNIFICANT OFF-DIAGONALS			
Element	Real Part	Imaginary Part	Improvement (percent closer to zero)
T_{71}	3.21650E-04	6.87400E-04	18.96
T_{62}	-9.89950E-08	-1.78470E-07	99.12
T_{84}	-3.02040E-18	8.25020E-19	100.00
T_{95}	1.18910E-07	-9.80070E-07	95.46
T_{26}	3.69920E-06	1.98190E-06	62.58
T_{17}	-5.87890E-04	1.30000E-03	79.74
T_{48}	9.56520E-07	2.56450E-07	98.07
T_{59}	2.68580E-04	1.18460E-04	97.69

Table IV. Significant Off-Diagonals.

C. FURTHER ANALYSIS AND DISCUSSION

Some Matrix algebra is employed to further characterize how well the T-Matrix off-diagonals were calculated. The following equation provides a normalization method used to characterize the off-diagonal elements relation to one.

$$\begin{bmatrix} \frac{1}{\sqrt{T_{11}}} & 0 & 0 & \cdots & 0 \\ 0 & \frac{1}{\sqrt{T_{22}}} & 0 & \cdots & 0 \\ 0 & & \ddots & \cdots & 0 \\ 0 & \cdots & 0 & & \frac{1}{\sqrt{T_{99}}} \end{bmatrix} \begin{bmatrix} T_{11} & & & \\ & T_{22} & & 0\text{'s \& errors} \\ & & \ddots & \\ 0\text{'s \& errors} & & & T_{88} \\ & & & & T_{99} \end{bmatrix} \begin{bmatrix} \frac{1}{\sqrt{T_{11}}} & 0 & 0 & \cdots & 0 \\ 0 & \frac{1}{\sqrt{T_{22}}} & 0 & \cdots & 0 \\ 0 & & \ddots & 0 \cdots & 0 \\ 0 & \cdots & 0 & & \frac{1}{\sqrt{T_{99}}} \end{bmatrix} \quad (24)$$

By multiplying both sides of the T-Matrix with the diagonal matrix as described in Equation (24) I will obtain

a matrix with one's along the diagonal and relative errors in the off-diagonal elements. By examining the magnitudes of the most significant off-diagonal elements, I can quickly gauge how "well" I calculated the T-Matrix. Again we see the same eight off-diagonals show the most significant levels with respect to the normalization. Although they are the most significant they are small. This method of analyzing the T-Matrix's off-diagonals provides a "quick-check" as to how well our numerical analysis is working. Table V provides our results for this analysis. Notice how small the magnitudes of these elements. All other elements have magnitudes on the order of element T_{84} and smaller.

T-MATRIX NORMALIZATION ANALYSIS (MOST SIGNIFICANT OFF-DIAGONALS)			
Element	Real Part	Imaginary Part	Magnitude
T_{71}	6.96163E-03	1.50759E-02	1.6606E-02
T_{62}	-2.65519E-06	-5.01816E-06	5.6773E-06
T_{84}	-8.44548E-17	2.12802E-17	8.7095E-17
T_{95}	5.96808E-05	1.55646E-05	6.1677E-05
T_{26}	1.01798E-04	5.71578E-05	1.1675E-04
T_{17}	-1.30097E-02	2.89475E-02	3.1737E-02
T_{48}	2.64606E-05	7.65933E-06	2.7547E-05
T_{59}	-9.58209E-03	1.56365E-02	1.8339E-02

Table V. T-Matrix Normalization Analysis.

(THIS PAGE INTENTIONALLY LEFT BLANK)

VI. CONCLUSION AND FOLLOW-ON PROPOSALS

A. CONCLUSION

I have derived an approximation for the self and mutual radiation impedances for spherical transducers of small *ka* values by considering two spheres in isolation. In this thesis, I have decided to call this approximation "Modal Pritchard". This approximation was tested for a general sphere of radius *a*=0.5 meters, frequency of 474 Hz, in water with sound speed of 1490 m/sec. Two general problems were tested: (1) two bodies radiating in three modes (monopoles, aligned dipoles, and aligned-linear quadrupoles) and (2) a three-body problem in which two bodies radiated in an array and the third acts as a moving scatterer. In all the two-body problems, the Modal Pritchard approximation provides mutual radiation impedance results close, if not exactly, matching the full Addition Theorem results. The same cannot be said for the three-body problem where scattering is important. Therefore, when scattering is important we recommend using the full Addition Theorem. In some cases, our Modal Pritchard approximation may be a useful tool in the design phase of low-frequency active sonars.

The numerical modeling portions of this thesis have updated and streamlined the process of calculating the scattering characteristics and T-matrix for an object under

study. Using a more refined mesh, only a partial improvement has been realized for the T-matrix calculation for a thin spherical-shell radiator. Unfortunately, current work showed worse errors for the monopole element of the T-Matrix.

We also noted some improvements in the calculation of the off-diagonal elements. Most off-diagonal elements showed an improvement of between 63 to 100 percent closer to zero as compared to previous work. I also provided a quick and easy means for determining how well we calculated the T-matrix off-diagonal elements by "normalizing" the matrix. With this process, we can quickly gauge the off-diagonal elements. As a result, seven off-diagonal elements were between 0.02 and 0.000006 as compared to the number one. All remaining off-diagonal elements (65) were smaller than $9.0*10^{-17}$ (most significantly smaller). Current work shows our T-matrix calculation was worse than previous work for the monopole element, but showed some improvements for other elements of the T-matrix. There is still room for further improvement which may be realized when ATILA radiation boundary problems are addressed.

B. FOLLOW-ON PROPOSALS

Further work with the "Modal Approximation" to the mutual radiation impedance include studying other problems such as arrays of multiple transducers and calculating the pressure field generated from their radiation. This investigation does not need to be limited to comparisons with computer generated results from the Addition Theorem. Follow-on work could use this Modal Pritchard approximation to compare with laboratory results of real transducers. With meticulous data gathering, one could study how well this approximation does in the "real" world.

As mentioned earlier, there continues to reside problems with the radiation boundary treatment in ATILA. This problem was to have been addressed with an even newer version of ATILA to include a tool called EQI. In reference to the second portion of this thesis, it is hoped that this modification will further improve the T-matrix calculation. Currently, about half of our T-matrix diagonal elements show magnitude errors below 7.3 percent and the rest are about 38 percent in error. Current phase errors are below 9 percent. Further analysis using the modified ATILA with EQI may reach our goal of relative errors below one percent. Future work could also use other refined meshes that may also provide further improvements.

(THIS PAGE INTENTIONALLY LEFT BLANK)

APPENDIX A: ADDITION THEOREM CALCULATION OF MUTUAL RADIATION IMPEDANCE

Here I will explain how I used the addition theorem to calculate the mutual radiation impedance for two identically hard spherical shells. I will refer to some equations in the text of this thesis throughout this explanation and will provide my MATLAB program along with some user defined functions.

Recall the application of the Addition Theorem to write the pressure from one sphere relative to the coordinate system of the other sphere, Equations (4) and (5) of the text. The application of the boundary conditions as written in Equation (6) brings us to Equations (8) and (9). I will rewrite the last two equations here.

$$\frac{-i\rho_o c V^{m_1}_{n_1}}{h'_{n_1}(ka)} = A^1_{n_1,m_1} + \left(\sum_{t_2=0}^{\infty} \sum_{s_2=-t_2}^{t_2} A^2_{t_2 s_2} \frac{j'_{n_1}(ka)}{h'_{n_1}(ka)} \sum_{\substack{p_1=|t_2-n_1| \\ p_1\geq|s_2-m_1|}}^{t_2+n_1} a(n_1,p_1,t_2,m_1,s_2) * h_{p_1}(kd)\Omega^{s_2-m_1}_{p_1}(\theta_{12},\phi_{12}) \right)$$

$$\frac{-i\rho_o c V^{m_2}_{n_2}}{h'_{n_2}(ka)} = A^2_{n_2,m_2} + \left(\sum_{t_1=0}^{\infty} \sum_{s_1=-t_1}^{t_1} A^1_{t_1 s_1} \frac{j'_{n_2}(ka)}{h'_{n_2}(ka)} \sum_{\substack{p_2=|t_1-n_2| \\ p_2\geq|s_1-m_2|}}^{t_1+n_2} a(n_2,p_2,t_1,m_2,s_1) * h_{p_2}(kd)\Omega^{s_1-m_2}_{p_2}(\pi-\theta_{12},\pi+\phi_{12}) \right).$$

These two equations are put into matrix form as given by Equation (10). Notice the infinity sign in the expression above. For practical purposes we have to truncate this infinity to some finite number *K*. Using *K* = 6, the left hand side of Equation (10) becomes a large 98 by 98 matrix multiplying a 98 element column vector for the left hand side and the right hand side is 98-element column vector with only two non-zero entries. We solve for the amplitudes in MATLAB by using a forward divide as follows.

$$\begin{bmatrix} I & B^1 \\ B^2 & I \end{bmatrix} \begin{bmatrix} \\ \vec{A} \\ \\ \end{bmatrix} = \begin{bmatrix} \vec{C}^1 \\ \vec{C}^2 \end{bmatrix} \quad where \quad \vec{A} = \begin{bmatrix} A^1 \\ A^2 \end{bmatrix}$$

With K = 6 the matrices have the following sizes,

$$\begin{bmatrix} \\ 98x98 \\ \\ \end{bmatrix} \begin{bmatrix} A's \\ 98x1 \end{bmatrix} = \begin{bmatrix} C^1 \\ C^2 \end{bmatrix} solving \begin{bmatrix} A's \\ \\ \end{bmatrix} = \begin{bmatrix} \\ 98x98 \\ \\ \end{bmatrix} / \begin{bmatrix} C^1 \\ C^2 \end{bmatrix}$$

Now we have solved the unknown A-coefficients and are ready to use these results to find the mutual radiation impedance.

Using Equation (13) with our solved A-coefficient values, we can easily solve for the radiation impedance,

given that the total radiation impedance can be written as $Z_{r1} = Z_{11} + Z_{12} * V_2 / V_1$. I first solve for the total radiation impedance by setting both V's equal to one. Then by setting $V_2 = 0$ I obtain the self-radiation impedance (Z_{11}) result. I then subtract Z_{11} from Z_{r1} to obtain the mutual-radiation impedance (Z_{12}) result.

Here are the MATLAB computer scripts used to generate these results along with all supporting user defined functions written for this analysis.

MAIN MATLAB PROGRAM

```
% Joseph L. Day
% Mutual impedance using the Addition Theorem
% 2 spheres along z-axis, with top sphere moving away
% Last updated July 27, 1999
format long
K=6;       % Truncated integer vice infinity
K2=(K+1)^2; % Useful number, it is the size of many vectors
k=2;        % Acoustic wave number.
radius=0.5;ka=k*radius;    % Both spheres with same radius.
theta=0;phi=pi;            % Angle from 2's origin to 1's
n1=0; m1=0; n2=0; m2=0;    % Defines the mode for each of the
two spheres
position1=1; % Position1 and Position2 are integers change
position2=1; % as follows: n1=0,m1=0 then position1=1;
             % n1=1,m1=-1 then position1=2; and
             % n1=1,m1=0 then position1=3,..and so on.
V1=1;V2=0;   % Spheres velocity amplitudes
             % Both equal to one gives Z(total)
             % With V1=1 and V2=0 gives Z11
speed=1490;  % speed of sound in the water.
rho=1000;    % density of the water.
temp1=eye(K2);temp2=zeros(K2,K2);
Big=[temp1 temp2;temp2 temp1];  % Matrix allocation
count=1;           % Initialize a counting process

for d=2.5:.25:24   % Distance with 0.25 meter increment
```

```
count1=1;count2=1; % Counting process.
Btemp1d=zeros(1,K2);
Btemp2d=zeros(1,K2);

for t=0:6

   for s=-t:t
      ptemp1a=abs(t-n1);ptemp1b=abs(s-m1);
      ptemp1c=max(ptemp1a,ptemp1b);
      ptemp2a=abs(t-n2);ptemp2b=abs(s-m2);
      ptemp2c=max(ptemp2a,ptemp2b);
      count3=1;count4=1;
      for p1=ptemp1c:2:t+n1
         M=s-m1;
         if p1<0
            P=(-1)^abs(M)*fact(p1-abs(M))/
             fact(p1+abs(M))*legendre(p1,cos(theta));
         else
            P=legendre(p1,cos(theta));
         end
         Btemp1a=a(n1,p1,t,m1,s)*shank2(p1,d);
         Btemp1b=P(1+abs(M))*exp(i*M*phi);
         Btemp1c(1,count3)=Btemp1a*Btemp1b;
         count3=count3+1;
      end

Btemp1d(1,count1)=sum(Btemp1c)*jprime(n1,ka)/hprime(n1,ka);
      count1=count1+1;
      for p2=ptemp2c:2:t+n2
         M=s-m2;
         if p2<0
            P=(-1)^abs(M)*fact(p2-abs(M))/
             fact(p2+abs(M))*legendre(p2,cos(theta-pi));
         else
            P=legendre(p2,cos(theta-pi));
         end
         Btemp2a=a(n2,p2,t,m2,s)*shank2(p2,d);
         Btemp2b=P(1+abs(M))*exp(i*M*(phi+pi));
         Btemp2c(1,count4)=Btemp2a*Btemp2b;
         count4=count4+1;
      end

Btemp2d(1,count2)=sum(Btemp2c)*jprime(n2,ka)/hprime(n2,ka);
      count2=count2+1;
   end
end
```

```
   Big(position1,K2+1:2*K2)=Btemp1d; %Placing values
   Big(K2+position2,1:K2)=Btemp2d;  %in the proper row.
   C(2*K2,1)=zeros;
   C(position1,1)=-i*rho*speed*V1/hprime(n1,ka);
   C(position2+K2,1)=-i*rho*speed*V2/hprime(n2,ka);
   A=Big\C;


Temporary=sum(conj(A(K2+1:2*K2,1))'.*Btemp1d*sbessj(n1,ka))*
          hprime(n1,ka)/jprime(n1,ka);
   Zr1=4*pi*radius^2/V1*(A(1,1)*shank2(n1,ka)+Temporary);
   Zrvector(count)=Zr1;
   count=count+1;
end

Zr1scaled=Zrvector/(4*pi*radius^2*rho*speed);

% This last value is the final answer and has been
% scaled for plotting purposes.
% Also for plotting purposes the final answer is calculated
% for ranges (d/a) from 2.5 to 24 in increments of 0.25.
% All plots were done using Microsoft Excel, since that
% program works better with Microsoft Word for cutting and
% pasting graphs.
```

Supporting user defined functions:

```
function A=a(s,t,r,u,m)

% computes the function a(s,t,r,u,m) of the Addition Theorem
%          as written in King and Van Buren

% Written by Joseph L. Day
num1=(2*s+1)*(2*t+1)*fact(s-u)*fact(t-
m+u)*fact(r+m)*fact((s+t+r)/2);
dem1=fact((r+t-s)/2)*fact((r+s-t)/2)*
     fact((s+t-r)/2)*fact(s+t+r+1);
term1=num1/dem1;
wmin=0.5*max([r-s-t,s-r-t-2*m+2*u,t-s-r+2*u]);
wmax=0.5*min([s+t-r,r+t-s-2*m+2*u,r+s-t+2*u]);
sum=0;
for w=wmin:wmax
   sum=sum+(-1)^w*bc(s+t-r,(s+t-r)/2+w)*
       bc(t+r-s,(t+r-s)/2+m-u+w)*bc(s+r-t,(s+r-t)/2-u+w);
end
A=real(i^(s+t-r))*term1*sum;  % Output from this function
```

```
function y=bc(n,m)

% Computes the binomial coefficient

% Written by Joseph L. Day
if m<0
   y=0;
elseif n-m<0
   y=0;
else
   y=prod(1:n)/(prod(1:m)*prod(1:n-m));
end
```

```
function y=fact(n)

% Computes the factorial of n
% Written by Joseph L. Day
y=prod(1:n);
```

```
function hn=shank2(n,x)

% Computes the Spherical Hankel function of the second kind
% Written by Joseph L. Day
hn=sqrt(pi/(2*x))*besselh(n+.5,2,x);
```

```
function jp=jprime(n,x)

% Computes the first derivative of the Spherical Bessel
%     function.
% Written by Joseph L. Day
jp=sqrt(pi/(2*x))*(besselj(n-.5,x)-
    (n+1)*besselj(n+.5,x)/(x));
```

```
function hp=hprime(n,x)

% Computes the first derivative of the Spherical Bessel
%          function.
% Written by Joseph L. Day
hp=sqrt(pi/(2*x))*(besselh(n-.5,2,x)-
       (n+1)*besselh(n+.5,2,x)/(x));
```

```
function jn=sbessj(n,x)

% Computes the Spherical Bessel function

% Written by Joseph L. Day
jn=sqrt(pi/(2*x))*besselj(n+.5,x);
```

(THIS PAGE INTENTIONALLY LEFT BLANK)

APPENDIX B: THREE-BODY ADDITION THEOREM CALCULATION

The solution for the mutual radiation impedance of the three-body problem as described in the Chapter III part B using the Addition Theorem is provided in this appendix. We start by writing the three radial velocities as expressed in Equation (2). The pressure from each of the three spheres (before we set sphere three as acoustically hard) can be expressed in the form of Equation (3).

As before we utilize the Addition Theorem to write the pressures from spheres 2 and 3 relative to sphere one (see Equation (4)). This gives us the expression for P_2^1 and P_3^1. The boundary conditions on the surface of each of the spheres leads to the following three equations.

$$V_1 = \frac{j}{\omega\rho_o}\frac{\partial}{\partial r}\left[P_1 + P_2^1 + P_3^1\right]\Big|_{r_1=a}$$

$$V_2 = \frac{j}{\omega\rho_o}\frac{\partial}{\partial r}\left[P_2 + P_1^2 + P_3^2\right]\Big|_{r_2=a}$$

$$V_2 = \frac{j}{\omega\rho_o}\frac{\partial}{\partial r}\left[P_3 + P_1^3 + P_2^3\right]\Big|_{r_2=a}$$

Then we obtain three big equations that are similar to Equations (7) and (8) each with an additional term. For example looking at Equation (7), the additional term will be much like the term in the parenthesis but will involve the coefficients for the third sphere (A^3).

Following a similar approach as used in Appendix A, we put our Equation (7)-type expressions in matrix form. We can write the following matrix relation.

$$\begin{bmatrix} I & B_2^1 & B_3^1 \\ B_1^2 & I & B_3^2 \\ B_1^3 & B_2^3 & I \end{bmatrix} \begin{bmatrix} \\ \vec{A} \\ \\ \end{bmatrix} = \begin{bmatrix} \vec{C}^1 \\ \vec{C}^2 \\ \vec{C}^2 \end{bmatrix} \quad where \quad \vec{A} = \begin{bmatrix} A^1 \\ A^2 \\ A^3 \end{bmatrix}$$

As before we will truncate the infinity value to $K = 6$ gives expression of the following sizes.

$$\begin{bmatrix} \\ 147x147 \\ \\ \end{bmatrix} \begin{bmatrix} A's \\ 147x1 \\ \\ \end{bmatrix} = \begin{bmatrix} C^1 \\ C^2 \\ C^3 \end{bmatrix} solving \begin{bmatrix} A's \\ \\ \\ \end{bmatrix} = \begin{bmatrix} \\ 147x147 \\ \\ \end{bmatrix} / \begin{bmatrix} C^1 \\ C^2 \\ C^3 \end{bmatrix}$$

We have solved for the three sphere coefficients and are now ready to complete our evaluation of the mutual radiation impedance. Using Equation (13) with these A-coefficients I can solve for the radiation impedance. Now I can write sphere one's total radiation impedance as $Z_{r1} = Z_{11} + Z_{12}*V_2/V_1+Z_{13}*V_3/V_1$. Now I make sphere three acoustically hard by setting the radial velocity amplitude in my computer code to zero. Next I solve for the total radiation impedance by setting sphere one and two's radial velocity amplitudes equal to one. I store this result and then calculate sphere one's self-radiation impedance by setting

sphere two's radial velocity amplitude to zero. I subtract this last result from the total radiation impedance, and that provides my mutual radiation impedance for sphere one due to all three spheres. The plotted data is calculated by incrementing the range of sphere three as it moves away from the two-sphere axis.

Here is the MATLAB computer code used to generate these results. All supporting functions have already been provided.

MATLAB Program for 3-body mutual radiation impedance

```
%  Written by Joseph L. Day
%  Mutual impedance using the Addition Theorem
%  Two spheres radiating, third (hard) sphere moving away
%  Last updated August 16, 1999
format long

K=6;       % Truncated integer vice infinity
K2=(K+1)^2;                 % A useful number
k=2;                        % waveNumber.
radius=0.5;ka=k*radius;     % for all three spheres
theta=0;phi=pi;             % Angle from 2's origin to 1's
n1=0; m1=0; n2=0; m2=0;     % Defines the mode for each sphere
n3=0; m3=0;
position1=1;                % Monopole position for matrices
position2=1;                % another monopole;
position3=1;                % like a monopole
V1=1;V2=1;V3=0;             % spheres velocity amplitudes
speed=1490;                 % speed of sound in the water
rho=1000;                   % density of the water

temp1=eye(K2);temp2=zeros(K2,K2);
Big=[temp1 temp2 temp2;temp2 temp1 temp2;temp2 temp2 temp1];
% setup some space for future calculation
count=1;                          % initialize a counting
process
phicheck=0;
```

```
for d=pi/2:.25:24          % Distance with 0.25 meter
increment
   d12=pi;
   count1a=1;count2a=1;count3a=1;% initialize counts.
   count1b=1;count2b=1;count3b=1;
   Btemp1da=zeros(1,K2);Btemp1db=zeros(1,K2);
   Btemp2da=zeros(1,K2);Btemp2db=zeros(1,K2);
   Btemp3da=zeros(1,K2);Btemp3db=zeros(1,K2);
   for t=0:6
      for s=-t:t
        ptemp1a=abs(t-n1);ptemp1b=
                abs(s-m1);ptemp1c=max(ptemp1a,ptemp1b);
        ptemp2a=abs(t-n2);ptemp2b=
                abs(s-m2);ptemp2c=max(ptemp2a,ptemp2b);
        ptemp3a=abs(t-n3);ptemp3b=
                abs(s-m3);ptemp3c=max(ptemp3a,ptemp3b);

count3=1;count4=1;count5=1;count6=1;count7=1;count8=1;
        for p1=ptemp1c:2:t+n1  %for B(1to2)
           M=s-m1;
           if p1<0
              P=(-1)^abs(M)*fact(p1-abs(M))/
                fact(p1+abs(M))*legendre(p1,cos(theta));
           else
              P=legendre(p1,cos(theta));
           end
           Btemp1a=a(n1,p1,t,m1,s)*shank2(p1,d12);
           Btemp1b=P(1+abs(M))*exp(i*M*phi);
           Btemp1c(1,count3)=Btemp1a*Btemp1b;
           count3=count3+1;
        end

       Btemp1da(1,count1a)=sum(Btemp1c)*jprime(n1,ka)/
                           hprime(n1,ka);
        count1a=count1a+1;
        phi13=pi/2+atan(pi/2/(d));
        theta13=3*pi/2;
        for p1=ptemp1c:2:t+n1  %for B(1to3)
           M=s-m1;
           if p1<0
              P=(-1)^abs(M)*fact(p1-abs(M))/
                fact(p1+abs(M))*legendre(p1,cos(theta13));
           else
              P=legendre(p1,cos(theta13));
           end
           d13=sqrt((pi/2)^2+(d)^2);
           Btemp1a=a(n1,p1,t,m1,s)*shank2(p1,d13);
```

```
    Btemp1b=P(1+abs(M))*exp(i*M*phi13);
    Btemp1c(1,count4)=Btemp1a*Btemp1b;
    count4=count4+1;
  end

Btemp1db(1,count1b)=sum(Btemp1c)*jprime(n1,ka)/
                    hprime(n1,ka);
  count1b=count1b+1;
  for p2=ptemp2c:2:t+n2 %for B(2to1)
    M=s-m2;
    if p2<0
      P=(-1)^abs(M)*fact(p2-bs(M))/fact(p2+abs(M))*
        legendre(p2,cos(theta-pi));
    else
      P=legendre(p2,cos(theta-pi));
    end
    Btemp2a=a(n2,p2,t,m2,s)*shank2(p2,d12);
    Btemp2b=P(1+abs(M))*exp(i*M*(phi+pi));
    Btemp2c(1,count5)=Btemp2a*Btemp2b;
    count5=count5+1;
  end

Btemp2da(1,count2a)=sum(Btemp2c)*jprime(n2,ka)/
                    hprime(n2,ka);
  count2a=count2a+1;
  phi23=pi/2-atan(pi/2/(d));
  theta23=3*pi/2;
  for p3=ptemp3c:2:t+n3  %for B(2,3)
    M=s-m3;
    if p3<0
      P=(-1)^abs(M)*fact(p3-abs(M))/
        fact(p3+abs(M))*legendre(p3,cos(theta23));
    else
      P=legendre(p3,cos(theta23));
    end
    d23=sqrt((pi/2)^2+(d)^2);
    Btemp3a=a(n3,p3,t,m3,s)*shank2(p3,d23);
    Btemp3b=P(1+abs(M))*exp(i*M*(phi23));
    Btemp3c(1,count6)=Btemp3a*Btemp3b;
    count6=count6+1;
  end

Btemp2db(1,count2b)=sum(Btemp3c)*jprime(n3,ka)/
                    hprime(n3,ka);
  count2b=count2b+1;
  for p3=ptemp3c:2:t+n3  %for B(3,1)
    M=s-m3;
```

```
            if p3<0
               P=(-1)^abs(M)*fact(p3-abs(M))/
               fact(p3+abs(M))*legendre(p3,cos(theta13-pi));
            else
               P=legendre(p3,cos(theta13-pi));
            end
            d23=sqrt((pi/2)^2+(d)^2);
            Btemp3a=a(n3,p3,t,m3,s)*shank2(p3,d13);
            Btemp3b=P(1+abs(M))*exp(i*M*(phi13+pi));
            Btemp3c(1,count7)=Btemp3a*Btemp3b;
            count7=count7+1;
         end

   Btemp3da(1,count3a)=sum(Btemp3c)*jprime(n3,ka)/
                       hprime(n3,ka);
         count3a=count3a+1;
         for p3=ptemp3c:2:t+n3  %for B(3,2)
            M=s-m3;
            if p3<0
               P=(-1)^abs(M)*fact(p3-abs(M))/
               fact(p3+abs(M))*legendre(p3,cos(theta23-pi));
            else
               P=legendre(p3,cos(theta23-pi));
            end
            Btemp3a=a(n3,p3,t,m3,s)*shank2(p3,d23);
            Btemp3b=P(1+abs(M))*exp(i*M*(phi23+pi));
            Btemp3c(1,count8)=Btemp3a*Btemp3b;
            count8=count8+1;
         end

      Btemp3db(1,count3b)=sum(Btemp3c)*jprime(n3,ka)/
                          hprime(n3,ka);
         count3b=count3b+1;
      end
      phicheck=phicheck+.25;
   end
   Big(position1,2*K2+1:3*K2)=Btemp1db;     % Placement
   Big(position1,K2+1:2*K2)=Btemp1da;
   Big(K2+position2,1:K2)=Btemp2da;         % of vectors.
   Big(K2+position2,2*K2+1:3*K2)=Btemp2db;
   Big(2*K2+position3,1:K2)=Btemp3da;
   Big(2*K2+position3,K2+1:2*K2)=Btemp3db;
   C(3*K2,1)=zeros;
   C(position1,1)=-i*rho*speed*V1/hprime(n1,ka);
   C(position2+K2,1)=-i*rho*speed*V2/hprime(n2,ka);
   C(position3+2*K2,1)=-i*rho*speed*V3/hprime(n3,ka);
   A=Big\C;
```

```
Temporary=sum(conj(A(K2+1:2*K2,1))'.*Btemp1da*sbessj(n1,ka))
*hprime(n1,ka)/jprime(n1,ka);

Temporary2=sum(conj(A(2*K2+1:3*K2,1))'.*Btemp1db*sbessj(n1,k
a))*hprime(n1,ka)/jprime(n1,ka);

Zr1=4*pi*radius^2/V1*(A(1,1)*shank2(n1,ka)+Temporary+Tempora
ry2);
   Zrvector(count)=Zr1;
   count=count+1;
end
Zr1scaled=Zrvector/(4*pi*radius^2*rho*speed);
```

(THIS PAGE INTENTIONALLY LEFT BLANK)

APPENDIX C: T-MATRIX CALCULATION

Upon obtaining the scattered pressures from the ATILA code for the user defined mesh, I then calculated the Transition Matrix (T-Matrix) for the user-defined transducer. For this analysis we used a thin spherical shell for our transducer.

Before I spell out my method for calculating the T-matrix, I should provide the reader with some background concerning this T-matrix (Ref. 3). First suppose the incident pressure to an object are standing spherical waves as represented by

$$p^{i}(r,\theta,\phi) = j_n(kr)\Omega_n^m(\theta,\varphi).$$

We use this T-matrix to transform from our incident pressure to the scattered pressure from the object subjected to this incident pressure. Basically, the T-Matrix describes the scattering property of each unique scatter (or in this case transducer) by using a discrete basis set of spherical harmonics. I determine the T-Matrix for my spherical shell by analyzing the scattering characteristics of this shell subject to a "standing" wave. Mathematically speaking, the T-matrix transforms our incident standing waves to scattered outgoing waves in the form of Hankel functions shown below.

$$p^r(r,\theta,\phi) = h_n(kr)\Omega_n^m(\theta,\varphi).$$

The following equation indicates the utility of the T-Matrix. The R_n values represent the reflection coefficients from the spherical shell and constitute elements of the T-Matrix.

$$\underbrace{\sum_n I_p j_p(kr)\Omega_p^m(\theta,\phi)}_{Standing\ Wave} \overset{T-Matrix}{\Rightarrow} \underbrace{\sum_n R_n h_n(kr)\Omega_n^m(\theta,\phi)}_{Radiating\ Wave}$$

Here is how I used these ideas to develop my T-matrix calculation. Starting with the output data from ATILA which is basically *N*-number of data points in the following form: for i = 1 to N we have x_i, y_i, z_i, and P_i. Then for all *N*-points I need to calculate the following product

$$h_n(r_i)\Omega_n^m(\theta_i,\varphi_i) = h_n(r_i \times k) \times P_n^m(\cos\theta_i) \times e^{im\phi_i}.$$

I will do this product up to the quadrupole, that is nine times for each n and m combination (n=0 and m=0, n=1 and m=-1, … n=2 and m=2). So for example if we have 100 data points, the number of calculated complex numbers is 900 (100 data points up to the quadrupole). The resulting matrix is of the form:

$$\begin{bmatrix} \textit{calculated complex numbers} \\ 100\ \textit{by}\ 9 \end{bmatrix} \begin{bmatrix} \uparrow \\ \vec{A} \\ (\textit{unknowns}) \\ (9x1) \\ \downarrow \end{bmatrix} = \begin{bmatrix} \uparrow \\ \text{Pressure} \\ (\textit{from ATILA}) \\ (100x1) \\ \downarrow \end{bmatrix}.$$

We solve for the unknown *A*-coefficients in MATLAB by the following equation [*A*] = [calculated numbers]\[*P*]. The forward divide sign in MATLAB is a solution for the *A* vector in a least squares sense to this over-determined system of equations [calculated numbers]*[*A*] = [*P*]. The effective rank of the calculated numbers matrix is determined from the QR decomposition with rank pivoting. The relationship of the T-matrix with the incident pressure amplitude vector [*B*] and the *A*-coefficients is as follows

$$\begin{bmatrix} T-matrix \end{bmatrix} \begin{bmatrix} B_{00} \\ B_{0-1} \\ B_{10} \\ \vdots \\ B_{22} \end{bmatrix} = \begin{bmatrix} A_{00} \\ A_{0-1} \\ A_{10} \\ \vdots \\ A_{22} \end{bmatrix}.$$

Since we obtain our results from ATILA for each n and m combination we solve for each column of the T-matrix in the following way. For example, we obtain ATILA's first scattering pressure results when we model the incident pressure with the standing waves using n=0 and m=0. We then use the scattering pressures to solve for the A-coefficients. Then we solve for the first column of the T-matrix by solving for the following equation.

$$\begin{bmatrix} & T & \end{bmatrix} \begin{bmatrix} 1 \\ 0 \\ 0 \\ \vdots \\ 0 \end{bmatrix} = \begin{bmatrix} A_{00} \\ A_{0-1} \\ A_{10} \\ \vdots \\ A_{22} \end{bmatrix}$$

Proceeding this way we can solve for all 9-columns of the T-matrix by changing the n and m values of the incident pressure accordingly. One final comment about this procedure to calculate the T-Matrix concerns the form of the incident wave. Because of certain limitations with the ATILA code we used a "traveling" wave vice the "standing" wave. The form of the incident pressure wave possible is a Hankel function instead of the spherical Bessel function. Because of this, a correction factor to the diagonal elements of 0.5*(diagonal element - 1) is necessary.

The following text provides the MATLAB program codes that I used to calculate the T-matrix. Also provided are

the user defined functions used in support of the main program and the analytical calculation for the T-matrix for thin spherical shells.

Main MATLAB Program:

```
% Joseph L. Day
% Calculation of the T-matrix
% last updated July 21, 1999

% Part 1: Import ATILA data and calculate the A coefficients
format long
data=getdata('temp5.dat');
% temp5.dat is a text file, tab deliminated with the first
% line as: number of rows, one-space, and number of columns.
% The data as follows: column 1: x; col. 2: y; col. 3: z;
% col. 4: real(pressure); and
% column 5: Imaginary(pressure).
x=data(:,1);y=data(:,2);z=data(:,3);
p=data(:,4)+i.*data(:,5);
k=2*pi*474/1492.94;        % since ka=1 and a=.5meters
count=1;   % initializes my count.
for N=0:2
   for M=-N:N
      Ptemp2=zeros(1,length(x));
      for n=1:length(x)
         r=sqrt((x(n))^2+(y(n))^2+(z(n))^2);
         theta=acos(z(n)/r);
         phi=atan2(y(n),x(n));
         if M<0
            P=(-1)^abs(M)*fact(N-abs(M))/
              fact(N+abs(M))*legendre(N,cos(theta));
         else
            P=legendre(N,cos(theta));
         end
         Ptemp1=shank2(N,k*r)*P(1+abs(M))*exp(i*M*phi);
         Ptemp2(n)=Ptemp1;
      end
      Ptemp2=(conj(Ptemp2))'; % make column vector
      eval(['Ptemp3' num2str(count) '=Ptemp2;']);
      count=count+1;
   end
end
```

```
cal=[Ptemp31 Ptemp32 Ptemp33 Ptemp34 Ptemp35 Ptemp36 Ptemp37
Ptemp38 Ptemp39];
% cal is a 100by9 matrix that will be used to determine
%      the A coefficients
A=cal\p;

% This final "A" value provides one column of the T-matrix.
% At this point I would apply the correction factor since
% we used a traveling wave instead of the standing wave.
% The n and m value determines which column of the T-matrix.
```

Supporting user defined functions:

```
function A=getdata(name)
%Function to read free-formated data A (matrix or vector)
% Written by Charles W. Therrien
if all(name ~= '.')
   name=[name,'.dat'];
end
[ft,message]=fopen(name,'r');
if ft<0
   error(message)
end
[bf,N]=fscanf(ft,'%g');
fclose(ft);
if bf(1)==N-1
   A=zeros(1,bf(1));
   A(:)=bf(2:N);
elseif bf(1)*bf(2)==N-2
   A=zeros(bf(2),bf(1));
   A(:)=bf(3:N);
   A=A.';
else
   A=bf.';
   fprintf([' Data length does not match count.\n',...
   ' File contents is being returned as a vector.\n'])
end
```

```
function hn=shank2(n,x)

% Computes the Spherical Hankel function of the second kind.
% Written by Joseph L. Day
hn=sqrt(pi/(2*x))*besselh(n+.5,2,x);
```

```
function y=fact(n)

% Computes the factorial of n
% Written by Joseph L. Day
y=prod(1:n);
```

Program to calculate the Analytical T-matrix for a thin spherical shell:

```
% Written by: Joseph L. Day
% Reference: ONR Report - AY98 Thesis (Ref 5)
% last updated April 6, 1999
% Computation of the T-matrix diagonal elements using
% the analytically derived formulas found (Ref 5, page 5).
format long
a=0.5;        % is the radius of the sphere in meters
h=0.01;       % is the shell thickness
E=215*10^9;   % is the bulk modulus in Pascals
v=0.33;       % is the Poisson's ratio shell's material
w=2*pi*474;   % is the angular frequency (474 Hz)
rhos=7500;    % is the density of the solid [kg/m^3]
rhof=1000;    % is the density of the fluid [kg/m^3]
cf=1492.94;   % is the sound speed of the fluid [m/s]
k=w/cf;       % is the wave number, in this case ka=1
cp=sqrt(E/(rhos*(1-v^2))); % plate wave speed
omega=w*a/cp;
M=1;
for N=0:2
   n=N;
   for m=-n:n
      b=omega^2-v-n*(n+1)+1;
      c=omega^2-2*(1+v);
      d=n*(n+1)*(1+v)^2;
      Z(M)=i*h*cp*rhos/(a*omega)*((b*c-d)/b);
      jn=sqrt(pi/(2*k*a))*besselj(n+.5,k*a);
      hn=sqrt(pi/(2*k*a))*besselh(n+.5,2,k*a);
      jhat=sqrt(pi/(2*k*a))*(besselj(n-.5,k*a)
           -(n+1)*besselj(n+.5,k*a)/(k*a));
      hhat=sqrt(pi/(2*k*a))*(besselh(n-.5,2,k*a)
           -(n+1)*besselh(n+.5,2,k*a)/(k*a));
      numerator=i*Z(M)*jhat+rhof*cf*jn;
```

```
        denom=i*Z(M)*hhat+rhof*cf*hn;
        T(M)=-numerator/denom;
        M=M+1;
    end
end
result=[(1:9)' real(T)' imag(T)' abs(T)' (angle(T)*180/pi)']
% result is the output: column 1: index number (n);
% column 2: real(T-matrix);
% column 3: image(T-matrix); column 4: amplitude;
% and column 5: phase (degrees).
```

LIST OF REFERENCES

1. Richards, R. T., Blottman III, J. B., and McTaggart, B., *Physics of Array Element Interaction Phenomena*, Proceedings of the International Workshop, held in Toulon France, pp. 86-108, June 1990.

2. Bentien, G. W., *Numerical Modeling of Array Interactions*, Proceedings of the International Workshop, held in Toulon France, pp. 109-124, June 1990.

3. Scandrett, C. L. and Baker, S. R., ONR Report on Array Modeling - AY98, 1998.

4. Kwon, Y. W. and Bang, H., The Finite Element Method using MATLAB, CRC Press LLC, 1997.

5. Ruiz, Arthur Lobo da Costa, *Calculation of the Transition Matrix for the Scattering of Acoustic Waves from a Thin Elastic Spherical Shell Using the ATILA Finite Element Code*, 1994.

6. Kinsler, L. E., Frey, A. R., Coppens, A. B. and Sanders, J. V., *Fundamentals of Acoustics*, John Wiley & Sons, 1982.

7. King, B. J., Van Buren, A. L., *A General Addition Theorem for Spheriodal Wave Functions*, SIAM Journal of Mathematical Analysis, Vol. 4, No. 1, pp. 149-160, February 1973.

8. New, R. and Eisler, T. J., Acoustic Radiation from Multiple Spheres, Journal of Sound and Vibration, Vol. 22, No. 1, pp. 1-17, 1973.

9. Abramowitz, M. and Stegun, I. A., *Handbook of Mathematical Functions with Formulas, Graphs, and Mathematical Tables*, Dover Publications, Inc., New York, 1970.

10. Pritchard, R. L., *Mutual Impedance Between Radiators in an Infinite Rigid Plane*, Journal of the Acoustical Society of America, Vol. 32, Number 6, pp. 730-737, June 1960.

11. Baker, S. R., and Scandrett, C. L., *Numerical Modeling of Sonar Transducers and Arrays*.

12. Scandrett, C. L., *Research Notes, September 1999*.

13. Institut Superieur d'Electronique du Nord (ISEN), ATILA Finite-Element Code for Piezoelectric and Magnetostrictive Transducer and Actuator Modeling Version 5.1.1, User's Manual, October 1997.

INITIAL DISTRIBUTION LIST

1. Defense Technical Information Center. 2
   8725 John J. Kingman Road, STE 0944
   Ft. Belvoir, VA 22060-6218

2. Dudley Knox Library 2
   Naval Postgraduate School
   411 Dyer Road
   Monterey, CA 93943-5101

3. Chairman, Department of Physics 1
   Code PH
   Naval Postgraduate School
   Monterey, CA 93943-5100

4. Prof. Steven R. Baker 1
   Code PH/Ba
   Naval Postgraduate School
   Monterey, CA 93943

5. Prof. Clyde L. Scandrett 1
   Code MA/Sd
   Naval Postgraduate School
   Monterey, CA 93943

6. Dr. Regis Bossut 1
   Institut Superieur d'Electronique du Nord
   41, Blvd. Vauban
   59046 Lille, Cedex, France

7. Office of Naval Intelligence 2
   ONI-11
   4251 Suitland Road
   Washington, D.C. 20395-5720

8. Joseph L. Day 1
   915 Sloan Ave.
   Waldorf, MD 20602

9. Mr. Jan Lindberg. 1
   Program Officer, Acoustic Transducers
   Office of Naval Research
   ONR 321, Sensors, Sources & Arrays
   800 North Quincy Street
   Arlington, VA 22217

10. Dr. Roger Richards 1
Code 2131 (Transducer Branch)
Naval Undersea Warfare Center
New London Detachment
New London, CT 06355-1644

11. Engineering & Technology Curricular Office 1
Code 34
Naval Postgraduate School
Monterey, CA 93943

12. George W. Benthien 1
Code D711
SPAWAR Systems Center, San Diego
53560 Hull Street
San Diego, CA 92152-5001